May 2020

Functionalization of 1,6,7,12-Tetrachloroperylene Tetracarboxylic Acid Anhydride for Synthesis of Metal-Organic Frameworks in Energy Applications

Andrei Palukoshka
Clemson University, palukoshka@gmail.com

FUNCTIONALIZATION OF 1,6,7,12-TETRACHLOROPERYLENE TETRACARBOXYLIC ACID ANHYDRIDE FOR SYNTHESIS OF METAL-ORGANIC FRAMEWORKS IN ENERGY APPLICATIONS

A Thesis
Presented to
the Graduate School of
Clemson University

In Partial Fulfillment
of the Requirements for the Degree
Master of Science
Chemistry

---

by
Andrei Palukoshka
May 2020

Accepted by:
Dr. Sourav Saha, Committee Chair
Dr. George Chumanov
Dr. Stephen Creager

ABSTRACT

1,6,7,12-tetrachloroperylene tetracarboxylic acid anhydride ($PDACl_4$) is a fluorescent dye with a wide range of tunability. This work explores the functionalization of $PDACl_4$ to exploit its supramolecular and photovoltaic (PV) capabilities. Synthesis of a novel pillared paddlewheel (PPW) metal-organic framework (MOF) using a bipyridyl functionalized tetrachloro perylene diimide ($BPyPDICl_4$) pillar with 2,6-naphthalenedicarboxylic acid (2,6-NDC) struts was successfully achieved and confirmed with X-ray diffraction (XRD). The growth of the new MOF as a thin film on both zinc oxide and titanium dioxide-coated fluorine-doped tin oxide (FTO) glass was explored for its potential use in dye-sensitized solar cell (DSSC) type application using powder x-ray diffraction (PXRD), UV-Vis, and diffuse reflectance (DR) spectroscopy. Other solvothermal syntheses of UiO, MOF-5, and PPF-type MOFs using tetrachloro perylene diimide ($PDICl_4$) ligands were performed and discussed. Organic synthesis of a new 4-tert-butylaniline based tetrachloro perylene diimide is reported along with its potential as a reaction intermediate. Bay substitution with cyclohexylamine, pyrrolidine, 1,2-dimethylhydrazie, 2-methoxyethanol, and pentaethylene glycol on various $PDICl_4$ derivatives is investigated through different synthetic routes with a final goal of substituting all four bay position with electron-rich or cation-coordinating moieties on a perylene diimide with metal-coordinating imide groups. Future direction for the novel MOF and the application of the newly synthesized PDI ligands in MOF application is discussed.

DEDICATION

1) I dedicate this work to my grandfather Stanislav Palukoshka, who passed away during my long academic journey. Although few, I have only happy memories of this man who was loved by many.

2) I dedicate this work to my parents, Viktar and Halina Palukoshka. They opened endless opportunities for their children by leaving everything behind and moving the family to America. They have always pushed me to achieve higher education.

3) I dedicate this work to Ashley Perkins. We fell into each other's orbit since the first day of graduate school and have been there ever since.

4) I dedicate this work to my close friends; Bhomesh, Ilya, and Chris. All of whom have taken the time to visit me at some point in Clemson during this taxing yet rewarding time.

ACKNOWLEDGMENTS

I thank Dr. Sourav Saha for his brilliant insights that laid the foundation for my research and the opportunity to work in his lab. I have learned many new techniques in his lab and gained much knowledge in the areas of supramolecular chemistry, organic synthesis, and MOF-incorporated device fabrication. More importantly he has taught me to approach scientific work in an effective and disciplined manner.

I thank Dr. Stephen Creager and Dr. George Chumanov for joining my committee. I also thank them for their mentorship in the classroom setting and the knowledge they have shared with me that has made this project possible.

I thank Dr. Colin McMillen for his spectacular work, both as a crystallographer and a teacher. He is responsible for collecting and refining X-ray diffraction data for the MOFs highlighted in this publication.

I thank Dr. James Plampin for his advice on teaching and organic synthesis. He is a personable supervisor with an elevated passion for chemistry who has a way of motivating other to care about it as much as he does.

I thank Krishnendu Maity and Dillip Panda for allowing me to contribute to their publication and showing me the ropes, as a first-year graduate student.

I thank my lab mates; Amina, Monica, Shiyu, Paola, Faysel, Ashok, and Suresh for their companionship and scientific insight.

TABLE OF CONTENTS

Page

Table of Contents (Continued)

Page

LIST OF FIGURES

LIST OF ABBREVIATIONS

1,1-DMH ..... 1,1-dimethyl hydrazine

1,2-DMH ..... 1,2-dimethyl hydrazine

2,6-NDC ..... 2,6-naphthalenedicarboxylic acid

4,4-BPDC ..... 4,4-biphenyldicarboxylic acid

AC ..... achiral

$BPyPDICl_4$ ..... bipyridyl tetrachloro perylene diimide (or ,N'-dipyridyl-1,6,7,12-tetrachloroperylene-3,4,9,10-tetracarboxylic acid diimide)

C_{60} ..... fullerene

$CDCl_3$ ..... deuterated chloroform

CH ..... cyclohexylamine

$CHCl_3$ ..... chloroform

CT ..... charge transfer

CV ..... cyclic voltammetry

DC ..... drop cast

DCM ..... dichloromethane

d-DCM ..... deuterated dichloromethane

d-DMSO ..... deuterated dimethylsufoxide

DEF ..... diethylformamide

DIPEA ..... diisopropylethylamine

DMF ..... dimethylformamide

List of Abbreviations (Continued)

DMSO ..... dimethylsulfoxide

DPNDI .dipyridylnaphthalenediiimide (or N'N'-di(4-pyridyl)-1,4,5,8-naphthalenediimide)

DR .....diffuse reflectance

DSSC ..... dye-sensitized solar cell

d-TFA.....deuterated trifluoroacetic acid

EtOH .....ethanol

FRET.....Forster (or fluorescence) energy transfer

FTO .....fluorine-doped tin oxide

H-NMR .....Hydrogen-nuclear magnetic resonance

HOMO ..... highest occupied molecular orbital

LBL ..... layer-bi-layer (deposition)

LUMO..... lowest unoccupied molecular orbital

M ..... minus

MALDI-TOF.....Matrix-assisted laser desorption-time of flight (mass spectrometry)

MeCN.....acetonitrile

MeOH .....methanol

MO .....metal oxide

MOF.....metal-organic framework

NDI .....naphthtalene diimide

NMP.....N-methyl-2-pyrrolidonen

List of Abbreviations (Continued)

n-octPDICl_4.....n-octyl tetrachloro perylene diimide (or N,N'-dioctyl-1,6,7,12 tetrachloroperylene-3,4,9,10-tetracarboxylic acid diimide)

OSC.....organic solar cell

P .....plus

PCE .....power conversion efficiency

PDA..... perylene dianhydride (or perylene-3,4,9,10-tetracrboxylic acid dianhydride)

PDACl_4. .....tetrachloro perylene dianhydride (or 1,6,7,12-Tetrachloroperylene tetracarboxylic acid dianhydride)

PDI .....perylene diimide (or perylene-3,4,9,10-tetracrboxylic acid diimide)

PDICl_4.. .....tetrachloro perylene diimide (or 1,6,7,12-Tetrachloroperylene tetracarboxylic acid diimide)

PDIPW ..... perylene diimide paddlewheel

PPF.....porphyrin paddlewheel

PPW .....pillar paddlewheel

PV .....photovoltaic

PXRD..... powder x-ray diffraction

SMA.....small molecule acceptors

SXRD.....single crystal x-ray diffraction

t-butBPDICl_4 ..... tert-butyl benzyl tetrachloro perylene diimid(or N,N'-di-4-tert-butyl benzyl-1,6,7,12-tetrachloroperylene-3,4,9,10-tetracarboxylic acid diimide)

List of Abbreviations (Continued)

TCPP ..... Tetrakis(4-carboxyphenyl)porphyrin

TFA ..... trifluoroacetic acid

UiO ..... University of Oslo

UV-vis ..... ultra violet-visual (light spectroscopy)

XRD ..... X-ray diffractiion

CHAPTER ONE

INTRODUCTION

Synthetic Background

In the last few decades, perylene, initially used as an industrial vat dye[1], has been researched and functionalized into perylene tetracarboxylic dianhydride (PDA) for its photonic potential, electron-deficient properties, supramolecular abilities, and tuneability.[2] The molecule is in the rylene family of dyes[3], which refers to molecules, made of two or more fused naphthalene molecules at the 1 and 8 positions of one naphthalene and the 4 and 5 of the other. Two naphthalene molecules fused in this configuration make perylene, which will be referred to as the perylene core.

PDA is synthesized from acenaphthene conversion to 1,8 naphthalene dicarboxylic acid anhydride by oxidation. This molecule is then turned to naphthalene-1,8-dicarboxylic acid imide, with the addition of ammonia. Molten KOH can couple the new naphthalene derivative at the 2 and 4 position to form the simplest perylene-3,4,9,10-tetracarboxylic diimide (PDI). Concentrated sulfuric acid is used to hydrolyze the PDI into PDA, the optimal starting material for further functionalization.[4]

PDA has three popular sites of functionalization. The anhydride portions are easily converted to imides with the addition of primary amines in acidic conditions. The perylene core portion of the molecule has 4 of each ortho and bay positions as seen in Figure 1.1. These positions can be functionalized with direct methods like alkylation and amination.[5,6,7] Electrophilic substitution of halogens may be done on the bay positions

with efficient yields. More specifically, chlorination of PDA into 1,6,7,12-tetrachloroperylene tetracarboxylic acid dianhydride ($PDACl_4$) can be practically achieved by adding chlorosulfanic acid and catalytic iodine.[1]

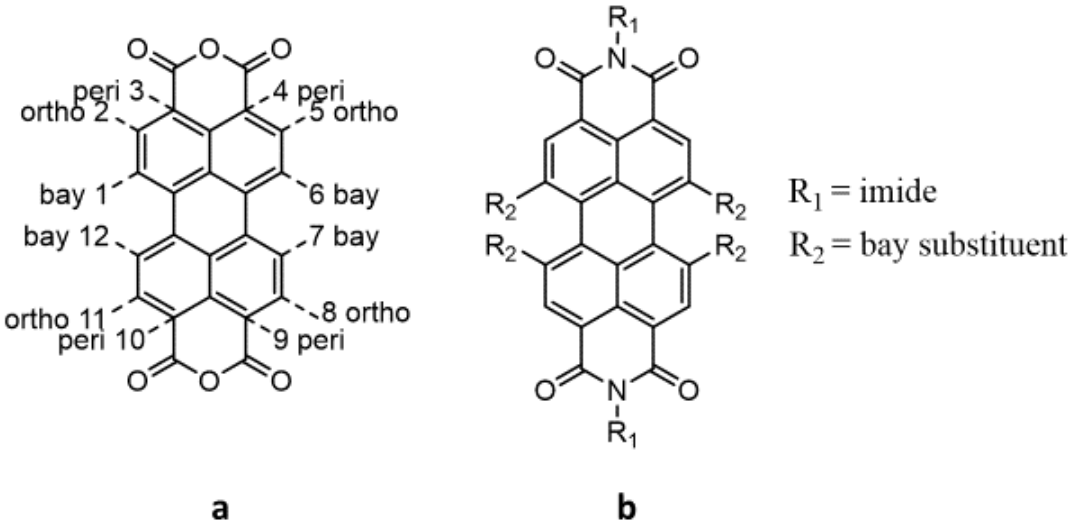

Figure 1.1 PDA and Bay-Functionalized PDI. a) Numbered positions od PDA. **b)** Full functionalization potential of $PDACl_4$.

Bay-halogenated PDIs allow for further functionalizing by substitution reactions. Among other less know groups the bay halogens can be replaced by amines, alcohols, thiols, fluoroalkyls, cyano groups, and via Suzuki coupling.[1] Unlike dibrominated PDIs, $PDICl_4$ does not have as much success in full bay replacement due to steric hindrance. The stress of the bay-substituents can be seen in the distortion of the perylene core plane, which has a torsion angle at its center, between the 1-12 bay positions and 6-7 bay positions. In the case of the molecule investigated in this work, $PDACl_4$, the torsion angle is 37 degrees.[8] For reference, the highest reported torsion angle is 42 degrees found in fused ring systems of the bay positions and the lowest angle of 1.5.[9,10] The imidization

and subsequent functionalization of a few significantly distorted $PDICl_4$s with amines and alcohols will be reported in this work.

$PDACl_4$ Tunability and Favorable Properties

Imidization of $PDACl_4$ is important for solubility and reactivity purposes, as $PDACl_4$ is only soluble with difficult solvents such as DMF and DMSO. Chlorinated solvents show some partial solubility as well. Solubility can increase with the imidization by aliphatic-containing amines. Imidization with functional groups such as pyridyl, carboxylic acid, sulfonic acid, et. can also allow for ligand to be metal-coordinating or allow it to anchor to thin film or glass surfaces such as zinc oxide, titanium dioxide, and quartz.[11] PDI aggregation through pi-stacking can be tuned with imidization but also through torsion angle alteration through bay position functionalization.

PDI ligands have not been explored in the MOF field extensively. The ligand is quite large and bulky. Bay-functionalized PDIs with a torsion angle have two non-superimposable isomers (M and P). A third AC variation has also been observed with alkoxy bay subsituents.[12] Enantiomeric mixture cause inconsistencies in supramolecular

aggregations as will be touched on in chapter 2.

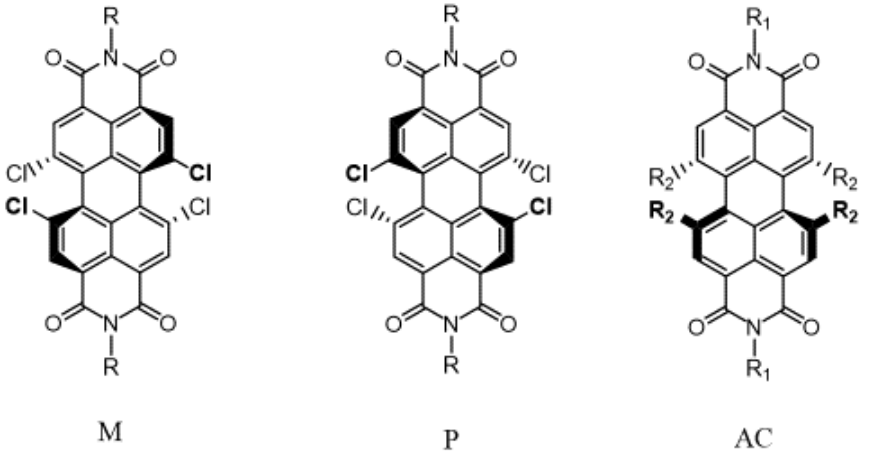

Figure 1.2 Enantiomeric Isomers of PDIs with Torsion. M is the minus propeller variation, **P** is the plus variation, and **AC** is achiral

In addition to the supramolecular tunability, PDIs offer more sought-after, tunable properties. To start, PDIs are dyes that can be functionalized to have color hues ranging from red to violet.[13] Although imidization has little to no change in the color due to the lack of HOMO LUMO overlap, bay-functionalization can be used to change the absorption/emission profiles. Due to their electron affinity, PDIs are excellent candidates for n-type semiconductors.[14] However, PDIs can also exhibit p-type behavior when both LUMO and HOMO levels are raised with the substitution of electron donating groups such as methoxy on the bay positions.[15] Generally, PDIs have high photostability and offer competitive fluorescence quantum yields, making them good candidates for light-induced energy transfer application in photonic devices.[14,16] Their electron-poor nature allows PDIs to be easily reduced and hard to oxidize, with unsubstituted PDIs having reduction potentials comparable to C_{60}, and $PDICl_4$ being an even stronger oxidant. The

electrodeficiency of the dyes gives them their photostability and allows them to avoid destructive photooxidation pathways, all while making them strong reductants in their excited state. This combination of properties allows for long-lived charge separated states in photoinduced electron transfer cascades.[17,18,14] However, in electron rich PDIs, reduction is disfavored, and reversible oxidation waves can appear at lower potentials in CV waves.[14] Although, these PDIs tend to absorb in the red, making them efficient in light harvesting when combined with the proper complementary ingredients.

PDIs' Potential Application in MOF-Based Solar Cells

PDIs have come a long way in organic solar cells (OSC). The highest power conversion efficiency (PCE) of a PDI related solar cell is 10.58% with the application of small molecule acceptors (SMAs).[19] However, this system involved a complicated synthesis, a tetrathiophene-based polymer, and relies on an optimized geometry of the PDI tetramer dye for efficient packing and good PCE. Additionally, PDIs have been used in more traditional dye-sensitized solar cells (DSSCs) with an optimal PCE of 2.6% and 1.1%, as a dyad.[20,21] The traditional DSSC mechanism starts with solar photons penetrating a transparent conductive glass, such as fluorine doped tin oxide (FTO), moving past a transparent metal-oxide anode (i.e. TiO_2 or ZnO) and exciting a metal-oxide (MO) attached dye such as PDI. The excited electron from the anode-anchored dye can then flow into the anode (leaving the dye oxidized) and then on to a cathode like platinum. The platinum counter electrode then reduces the electrolyte (redox mediator) I_3^- to $3I^-$, releasing two electrons and thereby quenching the previously-oxidized dye,

allowing $3I^-$ to return to I_3^-, completing the cycle and generating photocurrent. DSSCs are relatively new and have fair power conversion efficiencies (PCEs) as high as ~14.1%, according to (National Renewable Energy Laboratory) NREL. While this PCE is decent, there is still room to improve it. MOF-sensitized solar cells (MSSCs) offer room to improve DSSC performance by; expanding the range of light harvested to near IR, increasing open-circuit voltage, and reducing charge recombination.[24] In 2016, a PDI MOF-like film was introduced, and developed to operate with forester resonance energy transfer (FRET) properties. This film did not include PCE but showed the potential for absorbing a wide range of light.[22] Dye aggregation on the TiO_2 surface has been known to hinder open-circuit voltage, which can be avoided by uniform growth on the anode MO surfaces, which has been demonstrated on a ZnO surface with a porphyrin paddlewheel (PPF) MOF. [23]

This paper includes the synthesis of new PDI-based MOF. This new MOF is a fair scaffold for MSSCs. The growth of this MOF on MO surfaces is investigated along with its potential for harvesting light. Furthermore, the synthesis and bay-functionalization of a variety of PDIs is explored for their potential use in the substituting the PDICl4 ligand in the new MOF for PV or energy transfer applications. Lastly, future directions of PDI-PPF-based MOF synthesis and guest incorporation in the highlighted novel MOF is proposed.

REFERENCES

[1] Nowak-Król, A., & Würthner, F. (2019). Progress in the synthesis of perylene bisimide dyes. *Organic Chemistry Frontiers*, *6*(8), 1272-1318.

[2] Würthner, F. (2004). Perylene bisimide dyes as versatile building blocks for functional supramolecular architectures. *Chemical communications*, (14), 1564-1579.

[3] Heek, T., Würthner, F., & Haag, R. (2013). Synthesis and Optical Properties of Water-Soluble Polyglycerol-Dendronized Rylene Bisimide Dyes. *Chemistry–A European Journal*, *19*(33), 10911-10921.

[4] Huang, C., Barlow, S., & Marder, S. R. (2011). Perylene-3, 4, 9, 10-tetracarboxylic acid diimides: synthesis, physical properties, and use in organic electronics. *The Journal of organic chemistry*, *76*(8), 2386-2407.

[5] Yue, W., Li, Y., Jiang, W., Zhen, Y., & Wang, Z. (2009). Direct Meta-Selective Alkylation of Perylene Bisimides via Palladium-Catalyzed C− H Functionalization. *Organic letters*, *11*(23), 5430-5433.

[6] Schill, J., van Dun, S., Pouderoijen, M. J., Janssen, H. M., Milroy, L. G., Schenning, A. P., & Brunsveld, L. (2018). Synthesis and Self-Assembly of Bay-

Substituted Perylene Diimide Gemini-Type Surfactants as Off-On Fluorescent Probes for Lipid Bilayers. *Chemistry–A European Journal*, *24*(30), 7734-7741.

[7] Rauch, G., & Höger, S. (2014). N-Alkylated and N, N-dialkylated 1, 6-diaminoperylene diimides synthesized via copper catalyzed direct aromatic amination. *Chemical Communications*, *50*(42), 5659-5661.

[8] Li, X. Q., Stepanenko, V., Chen, Z., Prins, P., Siebbeles, L. D., & Würthner, F. (2006). Functional organogels from highly efficient organogelator based on perylene bisimide semiconductor. *Chemical communications*, (37), 3871-3873.

[9] Li, Z., Mo, Z., Meng, S., Gao, H., Niu, X., & Guo, R. (2016). The construction and application of chiral electrochemical sensors. *Analytical Methods*, *8*(46), 8134-8140.

[10] Jiménez, Á. J., Lin, M. J., Burschka, C., Becker, J., Settels, V., Engels, B., & Würthner, F. (2014). Structure–property relationships for 1, 7-diphenoxy-perylene bisimides in solution and in the solid state. *Chemical Science*, *5*(2), 608-619.

[11] Panda, D. K., Goodson, F. S., Ray, S., Lowell, R., & Saha, S. (2012). Multichromophoric dye-sensitized solar cells based on supramolecular zinc-

porphyrin⋯ perylene-imide dyads. *Chemical Communications*, *48*(70), 8775-8777.

[12] Nowak-Król, A., Roehr, M. I., Schmidt, D., & Würthner, F. (2017). A Crystalline π-Stack Containing Five Stereoisomers: Insights into Conformational Isomorphism, Chirality Inversion, and Disorder. *Angewandte Chemie*, *129*(39), 11936-11940.

[13] Herbst, W., & Hunger, K. (2006). *Industrial organic pigments: production, properties, applications*. John Wiley & Sons.

[14] Würthner, F. (2004). Perylene bisimide dyes as versatile building blocks for functional supramolecular architectures. *Chemical communications*, (14), 1564-1579.

[15] Leowanawat, P., Nowak-Król, A., & Würthner, F. (2016). Tetramethoxy-bay-substituted perylene bisimides by copper-mediated cross-coupling. *Organic Chemistry Frontiers*, *3*(5), 537-544.

[16] Battagliarin, G., Li, C., Enkelmann, V., & Müllen, K. (2011). 2, 5, 8, 11-Tetraboronic ester perylenediimides: a next generation building block for dye-stuff synthesis. *Organic letters*, *13*(12), 3012-3015.

[17] O'Neil, M. P., Niemczyk, M. P., Svec, W. A., Gosztola, D., Gaines, G. L., & Wasielewski, M. R. (1992). Picosecond optical switching based on biphotonic excitation of an electron donor-acceptor-donor molecule. *Science*, *257*(5066), 63-65.

[18] Prathapan, S., Yang, S. I., Seth, J., Miller, M. A., Bocian, D. F., Holten, D., & Lindsey, J. S. (2001). Synthesis and excited-state photodynamics of perylene− porphyrin dyads. 1. Parallel energy and charge transfer via a diphenylethyne linker. *The Journal of Physical Chemistry B*, *105*(34), 8237-8248.

[19] Zhang, J., Li, Y., Huang, J., Hu, H., Zhang, G., Ma, T., ... & Yan, H. (2017). Ring-fusion of perylene diimide acceptor enabling efficient nonfullerene organic solar cells with a small voltage loss. *Journal of the American Chemical Society*, *139*(45), 16092-16095.

[20] Panda, D. K., Goodson, F. S., Ray, S., Lowell, R., & Saha, S. (2012). Multichromophoric dye-sensitized solar cells based on supramolecular zinc-porphyrin⋯ perylene-imide dyads. *Chemical Communications*, *48*(70), 8775-8777.

[21] Shibano, Y., Umeyama, T., Matano, Y., & Imahori, H. (2007). Electron-donating perylene tetracarboxylic acids for dye-sensitized solar cells. *Organic Letters*, *9*(10), 1971-1974.

[22] Park, H. J., So, M. C., Gosztola, D., Wiederrecht, G. P., Emery, J. D., Martinson, A. B., ... & Stoddart, J. F. (2016). Layer-by-Layer Assembled Films of Perylene Diimide-and Squaraine-Containing Metal–Organic Framework-like Materials: Solar Energy Capture and Directional Energy Transfer. *ACS applied materials & interfaces*, *8*(38), 24983-24988.

[23] Gordillo, M. A., Panda, D. K., & Saha, S. (2018). Efficient MOF-Sensitized Solar Cells Featuring Solvothermally Grown [100]-Oriented Pillared Porphyrin Framework-11 Films on ZnO/FTO Surfaces. *ACS applied materials & interfaces*, *11*(3), 3196-3206.

[24] Spoerke, E. D., Small, L. J., Foster, M. E., Wheeler, J., Ullman, A. M., Stavila, V., ... & Allendorf, M. D. (2017). MOF-sensitized solar cells enabled by a pillared porphyrin framework. *The Journal of Physical Chemistry C*, *121*(9), 4816-4824.

CHAPTER TWO

PDI MOF SYNTHESES AND PDI MOF THIN-FILM GROWTH ON METAL-OXIDE SURFACES

$BAPDICl_4$ in MOF-5 and UiO

There is a growing amount of PV MOF publications but not as many that offer PCE values.[1,2] A few previously-published MOFs were considered to model a novel PDI MOF. MOF-5, a cubic framework with tetrahedral secondary binding units, was the first to be considered.[3] It was one of the earliest MOFs to be published and has a relatively simple synthesis. Hupp et al attempted and published a synthesis of this MOF using a benzoic acid functionalized $PDICl_4$ (**$BAPDICl_4$**) but failed to report XRD data said MOF.[4] The MOF was attempted due to the fact that it only has one ligand, which could also anchor to both ZnO and TiO_2 surfaces. The ligand was synthesized from $PDACl_4$ and followed by solvothermal synthesis, adapted to MOF-5 procedure. The resulting MOF can be seen in Figure 2.1.b. It can be seen that much of the **$BAPDICl_4$** was not dissolved but some very cubic crystals did form. The shape is a good indication of the synthesis but XRD was not pursued as the yield of the MOF was not promising due to the insolubility of **$BAPDICl_4$**.

Another considered template was from the UiO series. UiO MOFs are known to be very stable due to their Zr-O bonds. Although **$BAPDICl_4$** is much larger than the original BDC or BPDC ligands, it was believed that with interpenetration and strong Zr-O bonds, the structure could hold up. Conditions from literature were replicated and tuned a handful of times before moving on.[5] Attempts to replicate the cubic structure with

an enantiomeric mixture of ligand did not seem practical after a handful of attempts. Although not confirmed, the crude crystals were yielded in spherical shapes, as seen in Figure 2.1a. This shape has been indicative of fair crystallinity in cubic structures, due to non-uniform crystal growth along the cubic faces, growing out of the sides in a flattened, square-pyramidal fashion. Similar spheres were made in the initial attempts of MOF-5 like structures but the UiO materials were much finer.[4] With the UiO attempt yielding even worse qualitative results than the MOF-5 attempt, a different approach was considered.

Due to the enantiomeric nature of the chlorinated perylene core, $PDICl_4$ was reconsidered to be used as a pillar rather than a general linker with the imidization of 4-aminopyridine. The pyridine-based ligand, **$BPyPDICl_4$**, would also benefit PV devices because it would be easier to functionalize than the **$BAPDICl_4$** due to not having a carboxylic acid group to worry if bay functionalization is required. Additionally, only one equivalent of a **$BPyPDICl_4$** would be required for every two equivalents of strut. This ensures a higher likelihood of MOF formation because the 2-D strut sheets do not need to be enantiomerically pure. Brownian motion would then also ensure moving the correct M or P configuration of **$BPyPDICl_4$** to find its corresponding structure.

$BPyPDICl_4$ PPW MOFs

Previously-published NDI-based MOFs were considered as the model for the new PPW MOF due to the similarities that BPyNDI and BPyPDI ligands share. Both ligands are electron deficient and have similar solubility but vary in size. A couple

complementary struts were debated. 2,6-NDC and 4,4-BPDC were the first ligands considered because of their size, absorption profiles, and success with NDI PPW MOFs[6] **BPyPDICl$_4$** has absorption peaks from at 526nm, 491nm, and 430 nm (with decreasing peak intensity) and fluoresces at 554 nm.[7] 4,4-BPDC absorbs at 299 nm and again somewhere close to 250 nm.[8] 2,6-NDC absorbs in the UVA, UVB, and UVC region of the spectrum with peaks at 377 nm, 358 nm, 320 nm, 270 nm, and 206 nm.[9] The combined absorption spectra of 2,6-NDC and **BPyPDICl$_4$** absorb a significant portion of the UV-vis light with minimal, if any, overlap. Furthermore, the NDI NDC MOF was shown to be catenated and exhibit pi-pi charge transfer. This is important as it can undergo non-radiative charge recombination.[10] Successful synthesis of the 2,6-NDC **BPyPDICl$_4$** MOF was achieved by replacing NDI with **BPyPDICl$_4$** in the NDI NDC MOF procedure but also increasing the amount of DMF and time in the oven. The solvothermal synthesis, featured in Figure 2.2 was confirmed with SXRD. The new PDICl$_4$ paddle wheel MOF was named **PDIPW 1** as it is believed to be the first pillared paddle wheel PDI MOF to be reported with supporting XRD data.

PDIPW 1 is a 3-D MOF with a centrosymmetric space group of P-1. Currently, there are no XRD-confirmed PDICl$_4$ type MOFs in literature. It is possible that successful synthesis can be partially attributed to purification of the **BPyPDICl$_4$** ligand, which is highlighted in chapter 3. However, crystallographic structures, extrapolated from XRD data imply pi-aggregation of 2,6-NDC to half of the perylene core from the corresponding penetrating MOF.

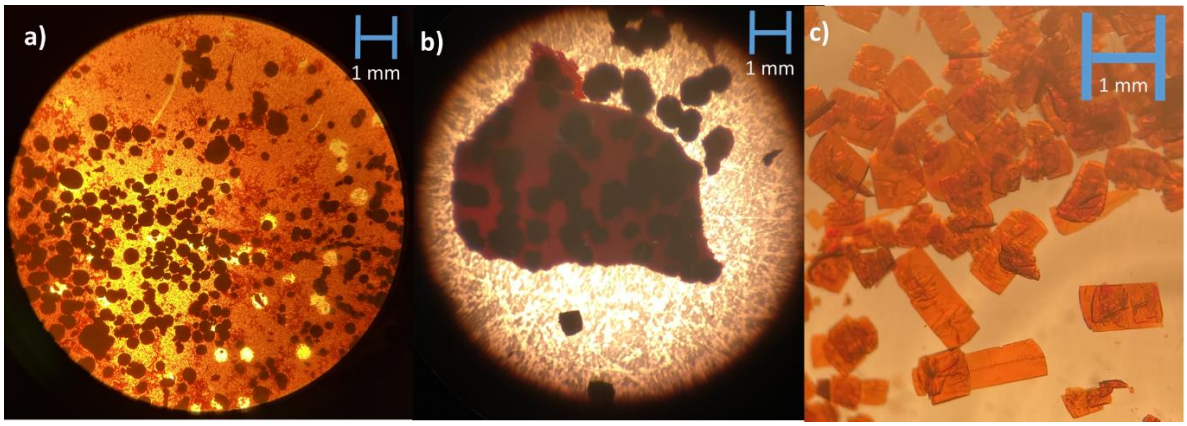

Figure 2.1 UiO-type PDI MOF, MOF-5-type PDI MOF, and **PDIPW 1** Under magnification. **a)** is the UiO type MOF, **b)** is the MOF-5 type MOF, **c)** is PDIPW 1. See Figure A-1 for distance scaling.

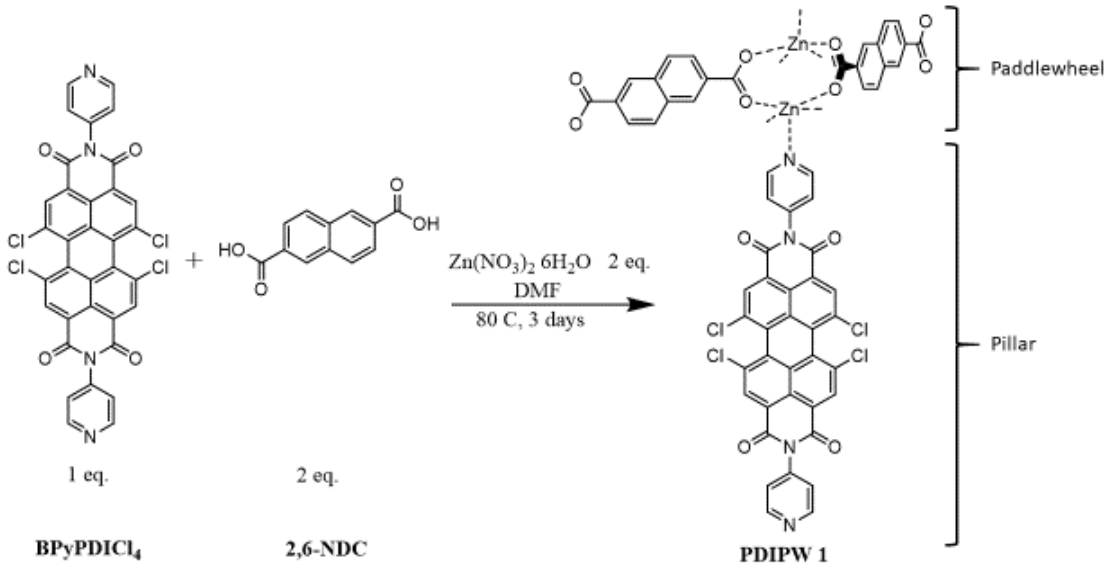

Figure 2.2 Solvothermal Synthesis of PDIPW 1. The paddlewheel portion of the MOF consists of four 2,6-NDC molecules surrounding two zinc atoms. The pillar coordinates the remaining Zn coordination sites, making the 2-D paddlewheel sheets into a 3-D structure.

This could give insight to the mechanism for the solvothermal synthesis and why this PDI MOF was successful, when so many others have failed. More importantly it shows potential for charge transfer as explored by Dinca in Hupp's DPNDI NDC MOF.[10]

At first glance of the packed unit cell, a 9.7 A distance is seen between the centers of the parallel perylene core and 2,6-NDC ligand (distance calculated in Figure A-2). However, as seen in Figure 2.3, repeating packed unit cells offer another pi-pi distance at 3.5 A which is indicative of pi-pi coordination. PDI is a fairly large and insoluble ligand that tends to aggregate with itself. This combined with PDI's insolubility can prevent or slow MOF formation. However, enantiomeric mixtures, orthogonal aromatic imide groups, and torsion angel can come together to suppress self-aggregation. More importantly, NDC offers pi-stacking competition, without hindering any metal cluster site formation, ultimately allowing the MOF to form.

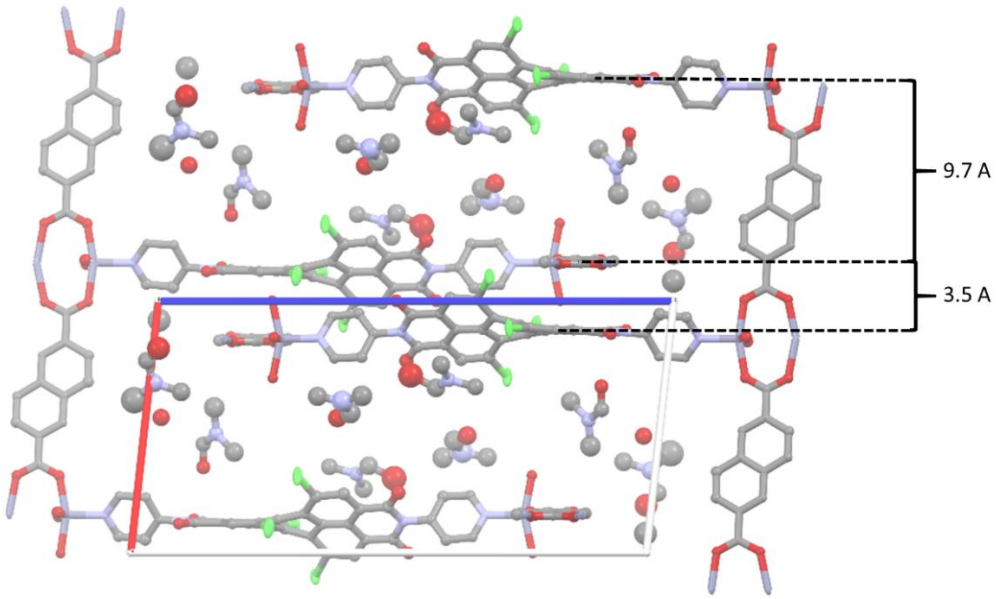

Figure 2.3. Repeated Packed Unit Cell of PDIPW 1. The unit cell is seen along the b-axis. The c-axis is the horizontal (white) and a-axis is vertically slanted (red).

MOF Growth on Metal-Oxide Surfaces

In previous studies, MOFs have been solvothermally grown on ZnO-coated FTO coated conductive glass surfaces to be used in light harvesting devices.[1,11] Both ZnO and TiO_2 can be coated on FTO glass for anchoring of carboxylates. However, pyridyl anchoring is much more likely to occur on TiO_2 with bulkier ligands.[12] Growing films on both TiO_2 and ZnO-coated FTO glass was attempted.

The first attempts were done by combining the **PDIPW 1** MOF reagents and solvent into a 20 mL vial, followed by either the TiO_2 or ZnO-coated FTO glass slide, angled with the coated side facing down. At the end of the synthesis, both vials had collected MOFs on the bottom of the vial and the glass slide consisted of spread-out sites where **PDIPW 1** nucleation happened (Figure 2.6a). This happened for both the ZnO and TiO_2-coated FTO glass and on both sides of the glass, with slightly more MOF growth on the TiO_2 slide. The ZnO-coated slide showed a yellow monolayer form on the ZnO-coated portion while the TiO_2 slide formed a reddish monolayer on the TiO_2 surface. Diffuse reflectance (DR) measurements were done on the blank TiO_2-FTO glass, followed by DR on the attempted MOF thin film device. The DR spectra confirmed that **BPyPDICl$_4$** was present due to the disappearance of the TiO_2-FTO peak at 390 nm with a couple of dips at the corresponding **BPyPDICl$_4$** absorption. The dips were confirmed with the Kubelka-Munk (KM) transform (Figure A-4). The newly-calculated PDI absorbance was blue shifted, suggesting that pi-pi stacking may be present. This would indicate that there is some level of MOF Growth on the surface and not just a monolayer of PDI. The blank DR measurement showed a lot alight being reflected and not scattered,

however with the PDIPW on the surface, the light is no longer lost to reflection but scattered into the material. Later normal absorbance spectra of a drop-casted (DC) MOF, on the TiO_2 side of FTO slide, was taken to get a reference of device that was not grown through anchoring.

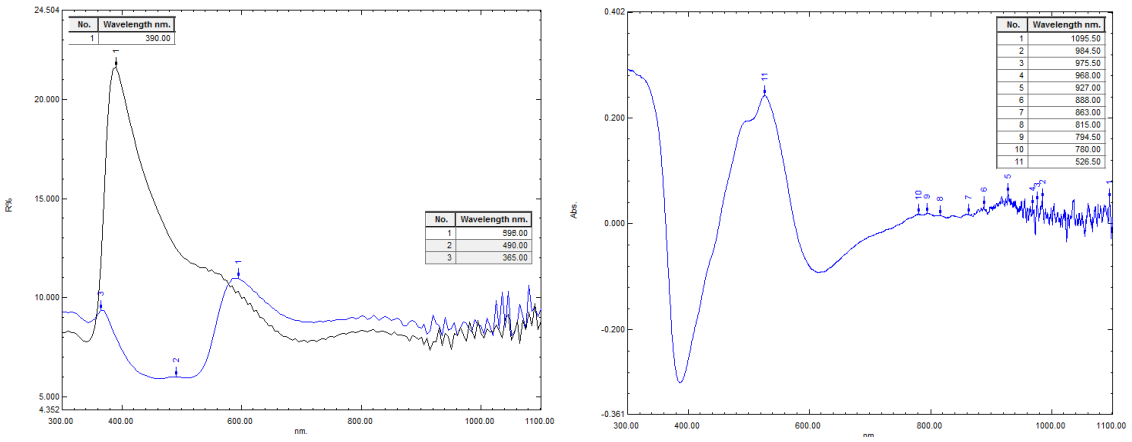

a **b**

Figure 2.4. DR and UV-vis of Three TiO_2-FTO Coated Glass Slide Variations. a) DR spectra of TiO_2-FTO blank slide (black) and grown **PDIPW 1** on TiO_2-FTO. **b)** Absorbance spectra from of DC PDIPW 1 TiO_2-FTO slide.

PXRD of the grown **PDIPW 1** TiO_2-FTO slide did not correspond to neither the simulated nor as synthesized spectra as seen in Figure 2.5. This may be due to the fact that the slide was placed directly into the instrument in place of a sample holder. However, the few peaks that were present also did not match up with the PXRD of TiO_2 nor the FTO literature values.[13] Although it should be noted that two of the peaks seem to be equally shifted to the left. If that is the case, then there may be stress between the grain boundaries, indicating the MOF was successfully anchored and grown from the surface.

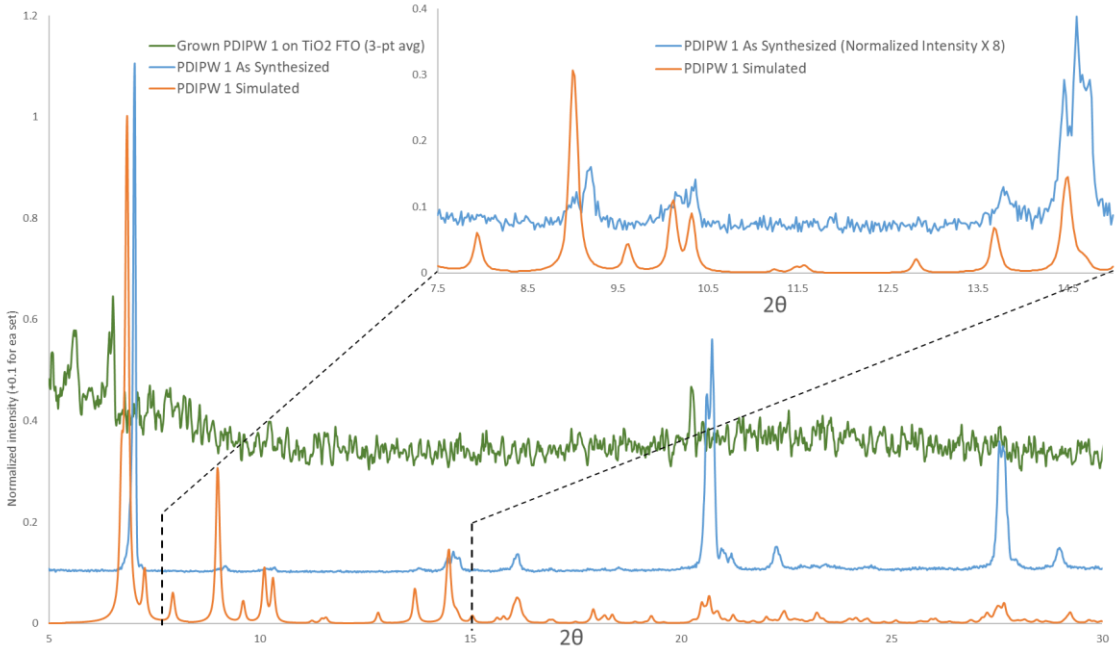

Figure 2.5. PXRD of Simulated PDIPW 1, as Synthesized PDIPW 1 and Grown PDIPW 1 on a TiO_2-FTO Surface. PXRD of PDIPW 1 'as simulated' is shown in orange. 'As synthesized' diffraction is shown in blue. This specific 'as synthesized' MOF was collected from the bottom of the vial used in the ZnO-FTO growing attempt pictures in Figure 2.6a. The 'as synthesized' intensity was increased by 8 times in the 7.5 to 15 (2θ) to show characteristic peaks from a low intensity region. Data of the grown **PDIPW 1** on TiO_2-FTO was adjusted with the 3-point averaging method and is shown in green (unaltered spectra and 3-point smoothing method can be found in Figure A-3).

Another approach to evenly grow the MOFs on the metal-oxide coated surfaces included adding the glass slide into the reaction vial a few hours after solvothermal synthesis was initiated to allow MOF microcrystals to form before so they could adhere to the surface. Also, pre-soaking a ZnO-FTO slide in 2,6-NDC and a TiO_2-FTO slide in **BPyPDICl$_4$** solutions was done to allow the ligands to orient themselves for growth. Figure 2.6b and Figure 2.6c show crystal growth on NDC-presoaked ZnO film and **BPyPDICl$_4$**-presoaked film. Unfortunately, most of the bulky crystals were easily washed from the surface with a soft DMF rinse.

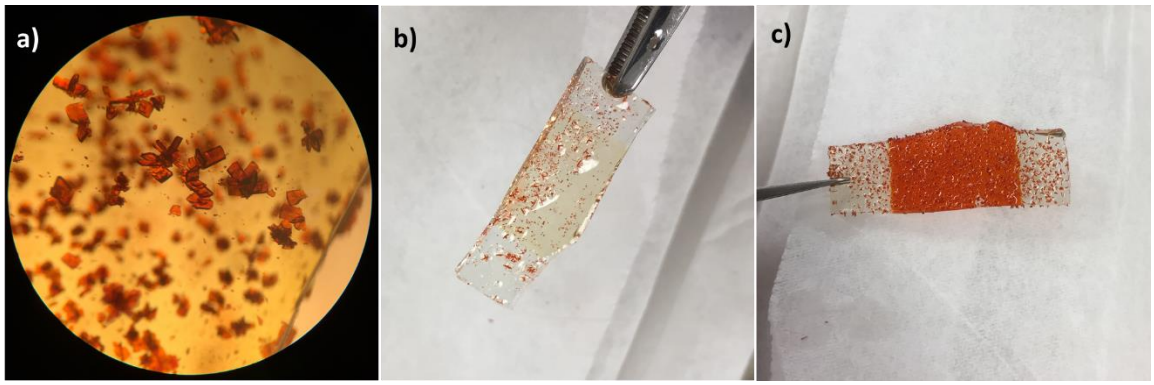

Figure 2.6. MOF Surface Growth on Glass Slides. a) PDIPW 1 growth on ZnO-FTO glass slide with no presoaking. **b)** ZnO-FTO that was presoaking in NDC solution before placing in initiated solvothermal synthesis vial. **c)** TiO_2 FTO slide that was presoaked in **BPyPDICl$_4$** solution before placing in a vial with preinitiated solvothermal synthesis.

As mentioned earlier, carboxylate coordination of TiO_2 with ZnO carboxylate is consistent with literature and TiO_2 has also been shown to anchor bulky pyridyl containing ligands.[1,10] This has been consistent with our findings so far. A mechanism for **PDIPW 1** can be proposed with these findings. If the pi-stacking between **BPyPDICl$_4$** and 2,6-NDC must occur first to suppress PDI-PDI pi-pi stacking and thereby starting MOF nucleation, then the MOF growth would be unlikely start with the 2,6-NDC as the anchored material, especially on the ZnO-coated surface because the distance between ZnO metal nodes is typically farther than that of the TiO_2. This would make orthogonal anchoring of the 2,6-NDC less likely than parallel anchoring (as if it to anchor with the paddlewheel flat on the surface). A parallel 2,6-NDC molecule would not have enough room for the PDI pi-stack to occur due to the pyridyl moiety being in the way. Even if the Zn nodes were close enough for carboxylate anchoring, the PDI would be too bulky to pi-coordinate to the anchored NDC. Another reason for the potential failure of the ZnO surface may be moisture from the air, which can form hydroxyl on the surface, forcing

carboxylates to find another site but also offering a new site for carbonyls to hydrogen bond to as the h-bond acceptor.

REFERENCES

[1] Gordillo, M. A., Panda, D. K., & Saha, S. (2018). Efficient MOF-Sensitized Solar Cells Featuring Solvothermally Grown [100]-Oriented Pillared Porphyrin Framework-11 Films on ZnO/FTO Surfaces. *ACS applied materials & interfaces*, *11*(3), 3196-3206.

[2] Park, H. J., So, M. C., Gosztola, D., Wiederrecht, G. P., Emery, J. D., Martinson, A. B., ... & Stoddart, J. F. (2016). Layer-by-Layer Assembled Films of Perylene Diimide-and Squaraine-Containing Metal–Organic Framework-like Materials: Solar Energy Capture and Directional Energy Transfer. *ACS applied materials & interfaces*, *8*(38), 24983-24988.

[3] Park, J. K., Han, Y. J., Lee, J. H., Joo, S. W., Kim, J. H., Lee, S. H., & Park, S. (2019). Characterization of the human head louse nit sheath reveals proteins with adhesive property that show no resemblance to known proteins. *Scientific reports*, *9*(1), 1-11.

[4] Nelson, A. P., Farha, O. K., Mulfort, K. L., & Hupp, J. T. (2009). Supercritical processing as a route to high internal surface areas and permanent microporosity in metal− organic framework materials. *Journal of the American Chemical Society*, *131*(2), 458-460.

[5] Kandiah, M., Nilsen, M. H., Usseglio, S., Jakobsen, S., Olsbye, U., Tilset, M., ... & Lillerud, K. P. (2010). Synthesis and stability of tagged UiO-66 Zr-MOFs. *Chemistry of Materials*, *22*(24), 6632-6640.

[6] Ma, B. Q., Mulfort, K. L., & Hupp, J. T. (2005). Microporous pillared paddle-wheel frameworks based on mixed-ligand coordination of zinc ions. *Inorganic chemistry*, *44*(14), 4912-4914.

[7] Troeger, A., Ledendecker, M., Margraf, J. T., Sgobba, V., Guldi, D. M., Vieweg, B. F., ... & Würthner, F. (2012). p-Doped Multiwall Carbon Nanotube/Perylene Diimide Derivative Photoelectrochemical Cells for Photocurrent Generation. *Advanced Energy Materials*, *2*(5), 536-540.

[8] Liu, Y. Y., Decadt, R., Bogaerts, T., Hemelsoet, K., Kaczmarek, A. M., Poelman, D., ... & Van Der Voort, P. (2013). Bipyridine-based nanosized metal–organic framework with tunable luminescence by a postmodification with Eu (III): an experimental and theoretical study. *The Journal of Physical Chemistry C*, *117*(21), 11302-11310.

[9] Gong, Y., Li, J., Qin, J., Wu, T., Cao, R., & Li, J. (2011). Metal (II) coordination polymers derived from bis-pyridyl-bis-amide ligands and carboxylates: syntheses,

topological structures, and photoluminescence properties. *Crystal growth & design*, *11*(5), 1662-1674.

[10] McCarthy, B. D., Hontz, E. R., Yost, S. R., Van Voorhis, T., & Dincă, M. (2013). Charge transfer or J-coupling? Assignment of an unexpected red-shifted absorption band in a naphthalenediimide-based metal–organic framework. *The journal of physical chemistry letters*, *4*(3), 453-458.

[11] Guo, Z., Panda, D. K., Maity, K., Lindsey, D., Parker, T. G., Albrecht-Schmitt, T. E., ... & Saha, S. (2016). Modulating the electrical conductivity of metal–organic framework films with intercalated guest π-systems. *Journal of Materials Chemistry C*, *4*(5), 894-899.

[12] Zhang, L., & Cole, J. M. (2015). Anchoring groups for dye-sensitized solar cells. *ACS applied materials & interfaces*, *7*(6), 3427-3455

[13] Zhou, Z., Yuan, S., Fan, J., Hou, Z., Zhou, W., Du, Z., & Wu, S. (2012). CuInS 2 quantum dot-sensitized TiO 2 nanorod array photoelectrodes: synthesis and performance optimization. *Nanoscale research letters*, *7*(1), 652.

CHAPTER THREE

PDACl$_4$ IMIDE FUNCTIONALIZATION AND PDICl$_4$ BAY SUBSTITUTION

General

As mentioned before, PDAs such as PDACl$_4$ can undergo imidization with a primary amine, in the presence of an acid. The imidizations done for this research can be found in Scheme 3.1. Imidization can be reversible in most cases and is done to increase the solubility, and therefore also the reactivity of the perylene molecule. These reactions more often than not offer fair to high yields. For example, the imidization of PDACl$_4$ with N-octylamine has a yield of 96%.[1] This variation of the PDACl$_4$ will be referred to as **n-octPDICl$_4$**. **N-octPDICl$_4$** has an aliphatic imide substituent that allows for substitution to occur at the chlorinated bay positions with little to no interaction with the imide. Once the substitution is complete, it is possible to return to the newly bay-functionalized PDA so that the desired coordinating group can be implemented for metal complexation.

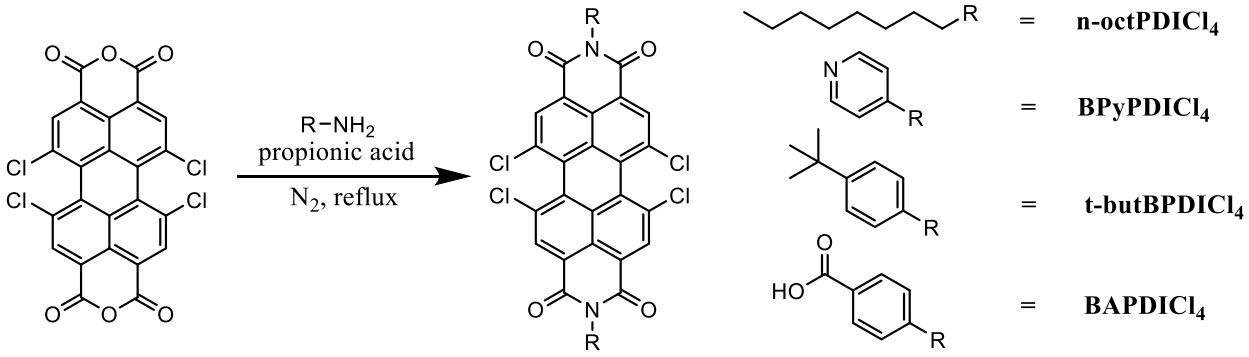

Scheme 3.1 Imidization of PDACl$_4$ into PDICl$_4$. These four imide substituents are referenced in this work.

Metal-Coordinating $PDICl_4$ Imide Substituents

In the case of **PDIPW 1** MOF, 4-aminopyridine was added as the new imide positions directly from $PDACl_4$. Previous aminopyridine imidizations of $PDACl_4$ were reported to have 31% and 98% yields.[2,3] A yield of 48% of **BPyPDICl_4** ligand was achieved after following the reaction time and equivalents of the latter procedure (98%) but only after column chromatography (1:99 MeOH:DCM), which was done in addition to the reported MeOH wash. It should be noted that the yield after the wash but before the column was recorded at close to 100%. The claim of a 98% yield is somewhat unlikely, as the H-NMR characterization was only confirmed with the addition of d-TFA. A DCM column was used in the 31% procedure. The highest attained yield following that procedure was 28% but only after adding and gradually increasing the percent of MeOH in $CHCl_3$ from 1 to 5% during column chromatography. With a DCM and or DCM:MeOH mobile phase, the yield was closer to 20%. Both literature procedures used some if not all d-TFA to characterize their ligand through H-NMR. While acid can help shift the peaks downfield from not overlapping with chloroform, it may also jeopardize the purity of the compound. As seen in Figure B-2, $CDCl_3$ can be used to characterize **BPyPDICl_4**. It is probable that synthesis of the robust MOF in Figure 2.1c was possible to this purity.

Novel t-butBPDICl_4

A novel 4-t-butylanaline functionalized $PDICl_4$ was also synthesized (**t-butBPDICl_4**) with a 34% yield (using only 2 eq. of 4-t-butylanaline) to explore the solubility of the molecule and offer an alternative to **oct-PDICl_4**. An unchlorinated t-

butBPDI has been reported with a 77.7% yield but under different reaction conditions. The t-butBPDI required 13.4 eq of t-butylanaline and a diethanolamine catalyst.[4] The use of a basic diethanolamine in addition to the already basic 4-t-butylanaline in a $PDICl_4$ systhesis would most likely show some substitution on the bay positions. Increasing the eq. of 4-t-butylanaline from 2 to 6 and decreacing propionic acid by 35% only showed an increase in a 4% yield to 38%. Although an increase in reaction time could potentially increase the yield significantly, further reaction optimization was halted as enough **t-butBPDI$_4$** was made for our means. **T-butBPDICl$_4$** offers tuning in fluorescence because, unlike other aryl imide PDIs, that have methyl or other alkyl groups in the imide ortho positions, t-butBPDICl_4 can undergo a "loose bolt" effect, where the aryl group is not anchored in place, decreasing the fluorescent yield due to vibronic motion.[5] However, this effect is applicable to **BPyPDICl$_4$** and **BAPDICl$_4$** so a more practical potential application for **t-butBPDICl$_4$** is as an intermediated in multistep synthesis of $PDICl_4$, because the H-NMR spectra is expected to show less interference in the alkyl region, compared to PDIs like **oct-PDICl$_4$**. This is crucial in characterizing alkyl-containing bay functionalization. Although, the potential of **t-butPDICl$_4$** as a common dye should not be ruled out.

Bay Substitution of $PDICl_4$

With the purified $PDICl_4$ derivatives in hand, bay functionalization could be explored in the aliphatic **n-octPDICl$_4$** or **t-butBPDICl$_4$** intermediate routes or direct functionalization of **BPyPDICl$_4$** and **BAPDICl$_4$.** In addition to alcohols, primary and secondary amines are decent candidates for this functionalization under basic conditions.

When deciding on an optimal synthesis for ligands to fit the **PDIPW 1** scaffold, three important criteria should be considered; **(i)** overall yield starting from the $PDACl_4$. The yield of **n-octPDICl$_4$** is 96%. with the addition of multiple steps, the final fully functionalized ligand yield can be expected to be significantly less. In previous example by Saha and coworkers, the 96% yielded **n-octPDICl$_4$** was bay substituted with t-butyl phenol, followed by deimidization back to a PDA with a yield of 72% after those few steps. A separate publication reported a 66% 4-aminopyridine imidization yield after that step to offer the best-case scenario yield from $PDACl_4$ to bay-functionalized BPyPDI of 48%. Coincidentally that is the experimental yield of the pure BPyPDICl4 ligand[6] **(ii)** Bay substituent purpose, reactivity, and purification potential are the next things that should be considered. There are 4 bay positions on the twisted perylene core. With each substitution, the torsion angle typically decreases, bringing sterics into the scene. Additionally, the reaction conditions become just slightly more acidic with the release of HCl after each substitution, lowering the reaction rate faintly. (**iii)** ligand size, stability, reactivity and solubility in solvothermal conditions must be accounted for as well. A large ligand is more likely to cause the MOF to collapse but also increases the chance of interpenetration if it is not too bulky. Because the ligand is being made for MOF synthesis, its stability in the presence of water from hydrous salts or slightly acidic conditions should be considered. Ligand solubility is also important because when it is used together with a ligand that is less soluble at different temperatures than the initial ligand.

Amine Bay Functionalization of $PDICl_4$

Because of **n-oct$PDICl_4$**'s impressive yield and solubility, it was considered as the first Aliphatic PDI to functionalize. As mentioned in chapter one, substitution on the bay positions will cause the substituent's (amine) HOMO to overlap with perylene LUMO causing the PDI exhibit a long-wave wavelength transfer band. This drives the fluorescence to be weaker and photostability is reduced.[7] The mechanism for amine bay-substitution of $PDICl_4$ has been somewhat debated. Three electron-rich amines were explored for bay functionalization; cyclohexylamine (a primary amine), a cyclic secondary amine known as pyrrolidine, and 1,2-dimethylhydrazine (DMH), which has two N-N bonded secondary amines (hydrazine functional group).

As a primary amine, cyclohexylamine (CH) has two hydrogens, which allows for multiple new bonds to form. After an amine has replaced one Cl on one side, the other chlorine may also be replaced. However, the site of nucleophilic attack could be somewhat hindered by the new CH substituent. A published reaction with 1,7-dibromo PDI showed 70% amine substitution but 30 % percent showed one-sided substitution with dehalogenation of the other bromine.[8] This information infers that there could be potential for the already substituted CH to let the same-sided Cl leave with its remaining proton, while forming another bond with that other bay position. The reaction was set over night in neat reflux conditions. After column chromatography, MALDI-TOF spectra (Figure B-9) agreed with this theory but H-NMR was less conclusive with the alkyl signals not lining up with the aromatic ortho protons.

Pyrrolidine has been successfully used in NDI based light-harvesting MOFs.[9] Under basic conditions, the substitution of the chlorines on the bay positions is possible. In the past, a tetrachloro PDI with 2,4-isopropyl benzene in the imide position was functionalized with pyrrolidine in neat conditions.[10] In the mentioned publication, two reactions were done. The first was in acetone, in an autoclave, at 160 C. The product was only characterized with TLC. The other reaction was in neat conditions, under N_2, at 55 C, and yielded only one substituted bay position. Neat conditions are a somewhat practical way to go about this. The acidic pKa of pyrrolidine is 35 so it is quite basic. The lone pair on the primary amine of the nucleophilic pyrrolidine is free to attack the bay carbon, which is meta directed by the withdrawing imide. The bulky nature of the substituent would make it difficult to substitute all the positions. However, $PDICl_4$ has one of the largest tortion angles and so imaginably, has a fair chance of substitution compared to a tetrabrominated PDI. Chromatography showed all variations of the substituted bay positions with MALDI-TOF. Eight fractions were collected, with little to no consistency in separation (Figure B-11). At this rate it was unlikely that the pyrrolidine product could rival the yield of direct substitution a **$BPyPDICl_4$**.

Another unattainable product in PDI reactions thus far, achieved through bay substitution, is the bridging substitution of diamine in the bay positions of one side. A diels-alder type reaction has been report on a non-halogenated PDI.[12] 1,2-dimethylhydrazine (DMH) was considered for such a task. A DMH 2HCl salt was purchased, (neat DMH is not practical due to its carcinogenic nature and instability in moist environments). Unlike 1,1-DMH, which has been known to be used as propellant,

1,2-DMH has little to no practical use, but would make for a good N-N donating group on the bay core of the molecule. It is also worth noting that non-methylated hydrazine is known to cleave imides, replacing that amine with itself. In this reaction, diisopropylethylamine (DIPEA) would be used as a proton scavenger as HCl is present on the DHM salt and is a byproduct. Although it is an amine, DIPEA cannot participate in the direct nucleophilic substitution due to its inaccessibility of the lone pair. Equivalents of the substituent where also considered due to the potential of polymerizing from the substitution of individual DMH on multiple PDI bay positions. Once the reaction was complete, MALDI-TOF showed promising spectra (Figure B-10) but H-NMR characterization showed to be difficult due to the alkyl proton overlap of the long n-octyl tails and methylamine substituents. To explore the substitution **t-butPDICl$_4$** was used because it offers a unique tetra-butyl alkyl group.

T-butBPDICl$_4$ was synthesized to confirm or deny potential substitution of DMH. **t-butBPDICl$_4$** has only one alkyl singlet H-NMR signal. While **n-octPDICl$_4$** has many. The t-butyl substituents can be used to gauge the product by looking at the splitting of the protons of the methyl groups. The reaction was attempted and H-NMR showed many peaks in the alkyl region as seen in Figure 3.2. This infers that there are a few variations of the t-butBPDI. This could mean that the hydrazine reacted with the imide positions or the bay positions. With 4 areas for substitution on the **t-butBPDICl$_4$** and two ways the DMH can substitute, there are 10+ variations of product. MALDI-TOF analysis was inconclusive as the mass of a practical variation was not confidently confirmed.

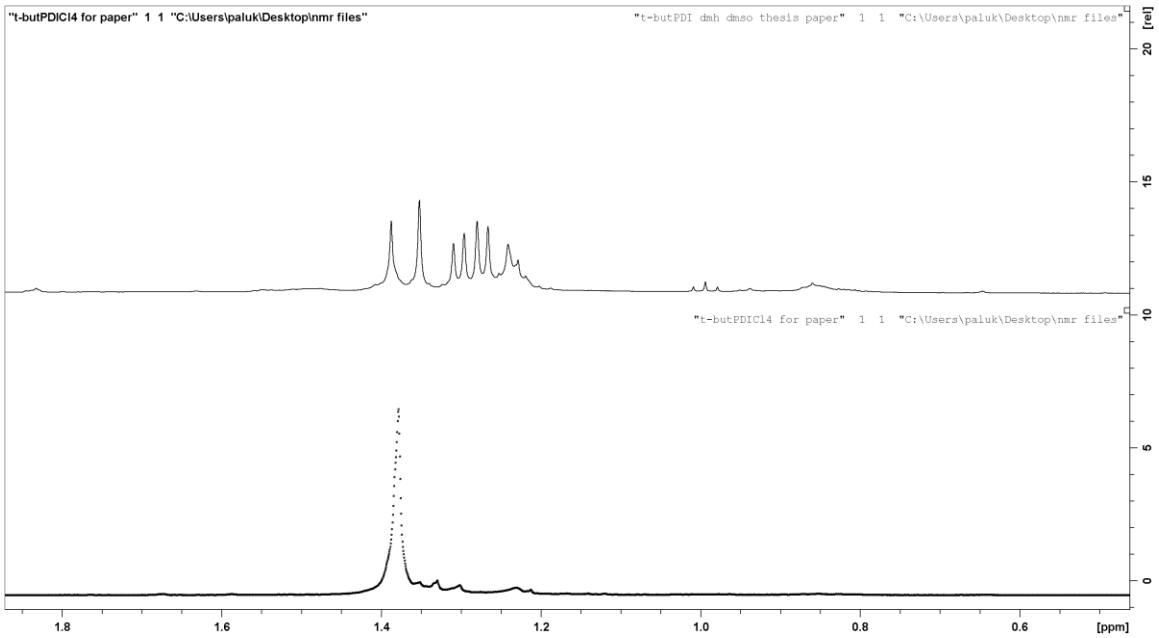

Figure 3.2. T-butyl as an NMR prob. The bottom spectra is **t-butBPDICl$_4$**, while the top is suspected to be DMH-functionalized. Splitting is generated between hydrogens in methyl groups.

Bay Functionalization of Metal-Coordinating BPyPDICl$_4$

Unlike the aliphatic PDIs, **BPyDICl$_4$** has pyridyl groups, containing potentially reactive lone pair that should be taken into consideration. Pyridyl substituents can pick up protons and make quartenary salts and have even been known to cleave. If the proper conditions could be addressed, direct substitution of the **BPyPDICl$_4$** ligand could potentially cut out two steps in the synthetic route to achieve a metal-coordinating PDI. DMH, pyrrolidine, and 2-methoxyethanol were used in this functionalization.

DMH functionalization of **BPyPDICl$_4$** was done a handful of times, varying the reaction times and reagent equivalents, while sticking to the reaction conditions, parallel to that of DMH functionalization of **n-octPDICl$_4$**. DMH and pyrrolidine did not show any characteristic MALDI peaks. Additionally, NMR showed quite a few inconsistencies

as well. Visual observation of color change can imply that photostability can also lead to impurities and unknown MALDI-TOF spectra peaks. Figure 3.3, below, shows the DMH functionalization of **BPyPDICl$_4$**. Upon dropwise addition of DIPEA to the charged reaction vessel, over the span of 10 minutes, the color began to turn green and then a mesmerizing blue. However, after 3 hours the reaction turned brown. Other attempts to aliquot these reactions ended with the aliquot turning that same brown hue once exposed to air. Photo degradation of perylene dyes upon exposure to oxygen has been reported before.[11]

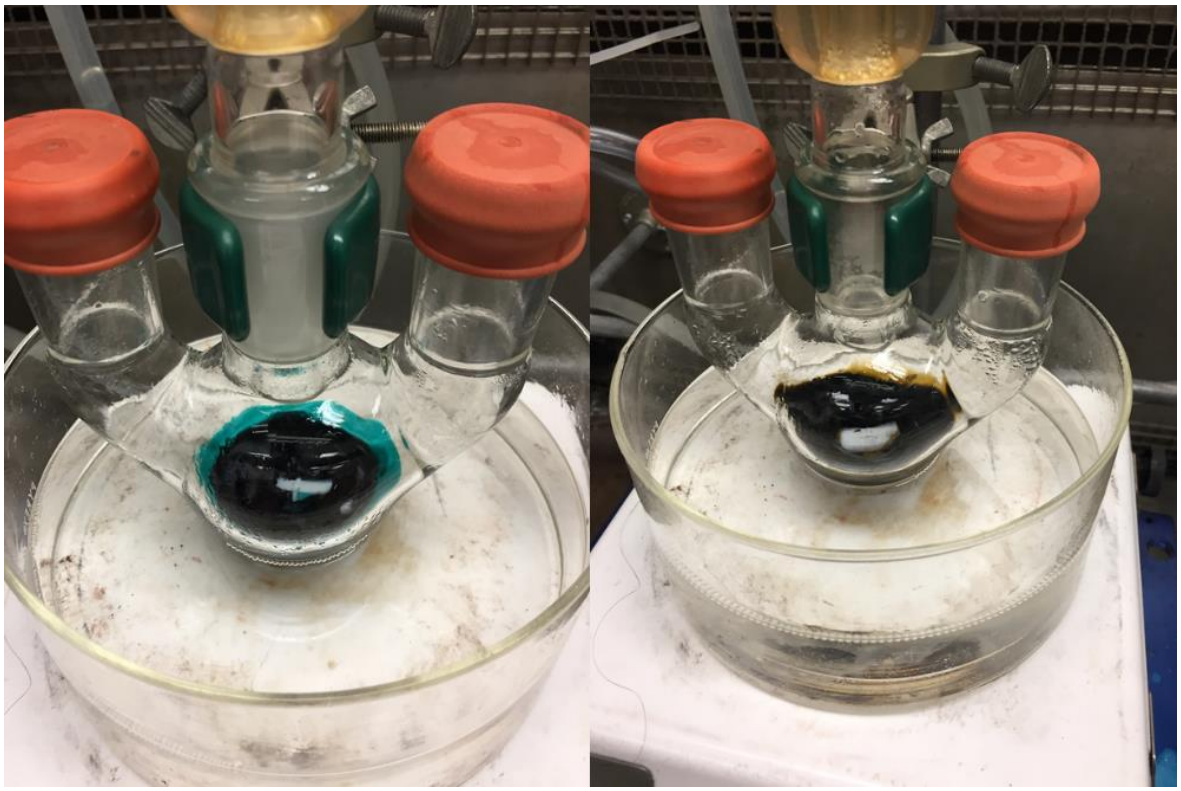

Figure 3.3. Photo Oxidation of During DMH Functionalized BPyPDICl$_4$

Ethylene Glycol Type Bay Functionalization

With amine functionalization starting to sound like a fragile option, functionalization of bay positions with ethylene glycols was introduced. There are a few untapped potentials in these positions for ethylene glycols. If functionalized properly, they can have the potential to bind a variety of different sized cations or act as hydrogen bond acceptors. 2-methoxyethanol, along with KCO_3 and DMF, has been used in bay functionalization in both n-octylPDI and BPyPDI, showing promising results, especially in the n-octPDI derivative.[13,14] Additionally, larger chains like pentaethylene glycol can be used to make a bay macrocycle. The coordinating potential can be seen below in Figure 3.3. MALDI-TOF spectra (Figure B-12,13,14) shows the promising potential of these compounds with the mass of the n-octPDI macrocycles already potentially having some small ion coordination.

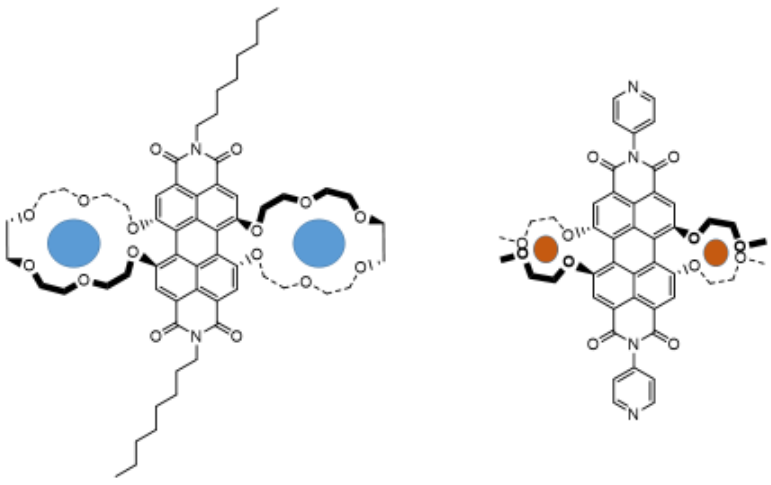

Figure 3.3. Coordinating Metal Ion Potential of PDI. The blue spots represent large cation and hydronium ion cooedination.[13,14]. Smaller metal cations like lithium are represented with the brown circles.

REFERENCES

[1] Panda, D. K., Goodson, F. S., Ray, S., Lowell, R., & Saha, S. (2012). Multichromophoric dye-sensitized solar cells based on supramolecular zinc-porphyrin⋯ perylene-imide dyads. *Chemical Communications*, *48*(70), 8775-8777.

[2] Troeger, A., Ledendecker, M., Margraf, J. T., Sgobba, V., Guldi, D. M., Vieweg, B. F., ... & Würthner, F. (2012). p-Doped Multiwall Carbon Nanotube/Perylene Diimide Derivative Photoelectrochemical Cells for Photocurrent Generation. *Advanced Energy Materials*, *2*(5), 536-540.

[3] Park, H. J., So, M. C., Gosztola, D., Wiederrecht, G. P., Emery, J. D., Martinson, A. B., ... & Stoddart, J. F. (2016). Layer-by-Layer Assembled Films of Perylene Diimide-and Squaraine-Containing Metal–Organic Framework-like Materials: Solar Energy Capture and Directional Energy Transfer. *ACS applied materials & interfaces*, *8*(38), 24983-24988.

[4] Cao, P., Khorev, O., Devaux, A., Sägesser, L., Kunzmann, A., Ecker, A., ... & Belser, P. (2016). Supramolecular organization of dye molecules in zeolite L channels: synthesis, properties, and composite materials. *Chemistry–A European Journal*, *22*(12), 4046-4060.

[5] Würthner, F. (2004). Perylene bisimide dyes as versatile building blocks for functional supramolecular architectures. *Chemical communications*, (14), 1564-1579.

[6] Würthner, F., Sautter, A., Schmid, D., & Weber, P. J. (2001). Fluorescent and electroactive cyclic assemblies from perylene tetracarboxylic acid bisimide ligands and metal phosphane triflates. *Chemistry–A European Journal*, *7*(4), 894-902.

[7] Nowak-Król, A., & Würthner, F. (2019). Progress in the synthesis of perylene bisimide dyes. *Organic Chemistry Frontiers*, *6*(8), 1272-1318.

[8] Zhao, C., Zhang, Y., Li, R., Li, X., & Jiang, J. (2007). Di (alkoxy)-and di (alkylthio)-substituted perylene-3, 4; 9, 10-tetracarboxy diimides with tunable electrochemical and photophysical properties. *The Journal of organic chemistry*, *72*(7), 2402-2410.

[9] Guo, Z., Panda, D. K., Maity, K., Lindsey, D., Parker, T. G., Albrecht-Schmitt, T. E., ... & Saha, S. (2016). Modulating the electrical conductivity of metal–organic framework films with intercalated guest π-systems. *Journal of Materials Chemistry C*, *4*(5), 894-899.

[10] Sun, M., He, Y., Ye, Y., Yang, W., & Yin, M. (2014). Nucleophilic substitution of tetrachloroperylene diimide in fluorescent polyvinylpyrrolidone film. *Macromolecular Chemistry and Physics*, *215*(6), 493-498.

[11] Tanaka, N., Barashkov, N., Heath, J., & Sisk, W. N. (2006). Photodegradation of polymer-dispersed perylene di-imide dyes. *Applied optics*, *45*(16), 3846-3851.

[12] Pandey, S. S., Inoue, T., Fujikawa, N., Yamaguchi, Y., & Hayase, S. (2010). Alkyl and fluoro-alkyl substituted squaraine dyes: A prospective approach towards development of novel NIR sensitizers. *Thin Solid Films*, *519*(3), 1066-1071.

[13] Buch-Pedersen, M. J., & Palmgren, M. G. (2003). Mechanism of proton transport by plant plasma membrane proton ATPases. *Journal of plant research*, *116*(6), 507-515.

[14] Steed, J. W. (2001). First-and second-sphere coordination chemistry of alkali metal crown ether complexes. *Coordination Chemistry Reviews*, *215*(1), 171-221.

CHAPTER FOUR

CONCLUSION AND FUTURE WORK

BPyPDICl$_4$ in PPF-TYPE MOFs and General Future Direction

Although PDICl$_4$ is powerful chromophore by itself, a complementary strut porphyrin ligand could increase PCE of a device substantially. The PPF (pillared porphyrin framework) series of MOFs has introduced a new type of light harvesting material. The PPF series of MOFs starts with PPF-1, which consist of stacked 2-D TCPP sheets.[1] The rest of the series is a variation of MOFs containing a variety of pillars that are either between two paddle wheels (like **PDIPW 1**) or between the porphyrin center metal and a paddlewheel.[2,3,4] PPF-11 was solvothermally grown on a ZnO-FTO surface to yield a PCE of 0.86%, which is competitive for MOF PV devices.[3,5] TCPP has an absorption maxima at 414 nm and at 422 nm when complexed with Zn in its center.[6] **BPyPDICl$_4$** has absorption peaks from at 526nm, 491nm, and 430 nm (with decreasing peak intensity.[7] The two complementary ligands have the potential to absorb much of the near UV spectrum. Functionalizing **BPyPDICl$_4$** will cause the absorbance to red shift, allowing even more of the spectrum to be utilized into power conversion.

The PFF-18,19, and 20 are all NDI-based MOFs.[4] Using the same strategy as before, replacing NDI with **BPyPDICl$_4$**, PPF-18, 19, and 20 variations were attempted, replacing DEF with DFM when needed. Many of the PPF syntheses require some ethanol and nitric acid to help with the Porphyrin. This could potentially protonate the pyridine on the **BPyPDICl$_4$**, stopping it from coordinating to metals. Additionally, recent novel

porphyrin MOFs are rather hard to characterize do the 2-D stacking of PPF-1 sheets. Some of these MOFs need extreme analytical techniques like a synchrotron.[8] Although all NDI-type approaches have failed, probably due to the catenation, enantiomeric nature of $PDICl_4$ and poor solubility, another angle has been considered. By Plugging the porphyrin center with a square planar d^8 platinum, pillar coordination will be limited to paddle wheels, much like the PPF-11 MOF. Pt coordination to the porphyrin center has been characterized with H-NMR and MALDI-TOF (Figure B-15 and B-16).

With the possible incorporation of porphyrin, higher PCE can be expected due to absorption of a wider range of UV-Vis light. Aside from the PPF or other new MOF approachs, **PDIPW 1** still has a lot to offer. With discovery of the tetra-methoxyethylene glycol BPyPDI and its potential incorporation into **PDIPW 1**, the MOF can be used in battery application, potentially even in tandem with the DSSC. Additionally, a variety of guests can be introduced to the **PDIPW 1** scaffold, as seen in doped MSSCs.[5,9] Also, other MO surfaces can be explored for anchoring and growing **PDIPW 1**. Other pi-stacking strut ligands can also be considered for PDIPW synthesis as well.

Conclusion

A novel PPW-type MOF was synthesized and confirmed through XRD methods Evident pi-stacking in the structure has been recognized for its pi-pi charge transfer possibility and potential role in the mechanism of the MOF formation. The MOF's growth on MO surfaces has been demonstrated along with drop casting. Diffuse reflectance and UV-Vis spectra was discussed along with the anchoring mechanism.

A novel **t-butBPDICl$_4$** molecule has been synthesized, offering an alternative intermediate in PDI bay substitution. Due to its fair solubility and sharp H-NMR signal, aliphatic bay functionalization can be monitored with less difficulty. Amine functionalization of PDI was most successful in **n-octPDICl$_4$** but did not show much photo stability, especially in aryl PDIs that are prone to the "loose bolt" effect. Ethylene glycol type substitution showed promising results with room to optimize reaction conditions.

REFERENCES

[1] Choi, E. Y., Wray, C. A., Hu, C., & Choe, W. (2009). Highly tunable metal–organic frameworks with open metal centers. *CrystEngComm*, *11*(4), 553-555.

[2] Choi, E. Y., Barron, P. M., Novotny, R. W., Son, H. T., Hu, C., & Choe, W. (2009). Pillared porphyrin homologous series: intergrowth in metal− organic frameworks. *Inorganic chemistry*, *48*(2), 426-428.

[3] Barron, P. M., Wray, C. A., Hu, C., Guo, Z., & Choe, W. (2010). A Bioinspired Synthetic Approach for Building Metal− Organic Frameworks with Accessible Metal Centers. *Inorganic chemistry*, *49*(22), 10217-10219.

[4] Chung, H., Barron, P. M., Novotny, R. W., Son, H. T., Hu, C., & Choe, W. (2009). Structural variation in porphyrin pillared homologous series: influence of distinct coordination centers for pillars on framework topology. *Crystal Growth and Design*, *9*(7), 3327-3332.

[5] Gordillo, M. A., Panda, D. K., & Saha, S. (2018). Efficient MOF-Sensitized Solar Cells Featuring Solvothermally Grown [100]-Oriented Pillared Porphyrin Framework-11 Films on ZnO/FTO Surfaces. *ACS applied materials & interfaces*, *11*(3), 3196-3206.

[6] La, D. D., Rananaware, A., Thi, H. P. N., Jones, L., & Bhosale, S. V. (2017). Fabrication of a TiO2@ porphyrin nanofiber hybrid material: a highly efficient photocatalyst under simulated sunlight irradiation. *Advances in Natural Sciences: Nanoscience and Nanotechnology*, *8*(1), 015009.

[7] Troeger, A., Ledendecker, M., Margraf, J. T., Sgobba, V., Guldi, D. M., Vieweg, B. F., ... & Würthner, F. (2012). p-Doped Multiwall Carbon Nanotube/Perylene Diimide Derivative Photoelectrochemical Cells for Photocurrent Generation. *Advanced Energy Materials*, *2*(5), 536-540.

[8] Williams, D. E., Rietman, J. A., Maier, J. M., Tan, R., Greytak, A. B., Smith, M. D., ... & Shustova, N. B. (2014). Energy Transfer on Demand: Photoswitch-Directed Behavior of Metal–Porphyrin Frameworks. *Journal of the American Chemical Society*, *136*(34), 11886-11889.

[9] Guo, Z., Panda, D. K., Maity, K., Lindsey, D., Parker, T. G., Albrecht-Schmitt, T. E., ... & Saha, S. (2016). Modulating the electrical conductivity of metal–organic framework films with intercalated guest π-systems. *Journal of Materials Chemistry C*, *4*(5), 894-899.

APPENDICES

Appendix A

PDIPW 1 Crystallography Data

XRD

Title

q-1051_a.res in P-1

Crystal data

Formula sum	$Zn_4\ Cl_8\ O_{30}\ N_{13}\ C_{133}$
Formula weight	2804.71
Crystal system	triclinic
Space group	*P* -1 (no. 2)
Unit cell dimensions	*a* = 13.0594(13) Å
	b = 13.1125(13) Å
	c = 26.5379(25) Å
	α = 95.58(0) °
	β = 95.46(0) °
	γ = 97.16(0) °
Cell volume	4460.97(291) $Å^3$
Density, calculated	1.044 g/cm^3
Pearson code	aP205
Formula type	N4O8P13Q30R133
Wyckoff sequence	i^{102}

Atomic coordinates and isotropic displacement parameters (in Å ^{2})

Atom	Wyck.	Occ.	x	y	z	U
TWIN	1*a*	0	-1.00000	0	-1.00000	0.0000
ZN1	2*i*		0.84974	0.77028	-0.13406	
ZN2	2*i*		0.84888	0.76525	0.75539	
CL1	2*i*		0.90295	0.45664	0.26237	
CL2	2*i*		0.89104	1.05414	0.31403	
CL3	2*i*		0.69655	0.48589	0.30698	
CL4	2*i*		1.09701	0.99288	0.36270	
O1	2*i*		0.69494	0.75575	-0.15509	0.0327
O2	2*i*		0.69342	0.75618	-0.23829	0.0301
O3	2*i*		0.00337	0.77900	-0.22061	0.0268
O4	2*i*		0.00337	0.77652	-0.13645	0.0272
O5	2*i*		0.84010	0.61383	0.76556	0.0434
O6	2*i*		0.84041	0.61215	0.84897	0.0421
O7	2*i*		0.85547	-0.08026	0.76792	0.0328
O8	2*i*		0.85718	-0.07872	0.85195	0.0370
O9	2*i*		0.88556	0.61076	0.08641	0.0361
O10	2*i*		0.86905	0.95376	0.11512	0.0396
O11	2*i*		0.76256	0.58421	0.50604	0.0592
O12	2*i*		1.00179	0.87160	0.53890	0.0454
N1	2*i*		0.85161	0.78535	-0.05794	0.0234
N2	2*i*		0.87736	0.78142	0.10106	0.0232
N3	2*i*		0.87697	0.72814	0.52203	0.0335
N4	2*i*		0.85255	0.74675	0.67952	0.0236
C1	2*i*		0.64881	0.75822	-0.19839	0.0247

Atom	Wyck.	Occ.	x	y	z	U
C2	2*i*		0.53619	0.76329	-0.20290	0.0215
C3	2*i*		0.48439	0.75988	-0.16023	0.0223
C4	2*i*		0.37754	0.76525	-0.16293	0.0256
C5	2*i*		0.32193	0.77462	-0.21119	0.0207
C6	2*i*		0.37908	0.77713	-0.25396	0.0273
C7	2*i*		0.48198	0.77134	-0.25068	0.0328
C8	2*i*		0.32083	0.76348	-0.11922	0.0359
C9	2*i*		0.21651	0.76846	-0.12383	0.0319
C10	2*i*		0.16234	0.77776	-0.17171	0.0166
C11	2*i*		0.21632	0.78103	-0.21417	0.0198
C12	2*i*		0.04888	0.77863	-0.17557	0.0155
C13	2*i*		0.83998	0.57082	0.80392	0.0323
C14	2*i*		0.84088	0.45320	0.79755	0.0330
C15	2*i*		0.84403	0.40377	0.74783	0.0417
C16	2*i*		0.84834	0.29812	0.74073	0.0428
C17	2*i*		0.84887	0.24494	0.78336	0.0308
C18	2*i*		0.84444	0.28985	0.83315	0.0285
C19	2*i*		0.84048	0.40075	0.83817	0.0349
C20	2*i*		0.85158	0.13136	0.77655	0.0338
C21	2*i*		0.85090	0.07739	0.81781	0.0276
C22	2*i*		0.84644	0.12940	0.86781	0.0373
C23	2*i*		0.84356	0.23348	0.87392	0.0386
C24	2*i*		0.85491	-0.03692	0.81133	0.0225
C25	2*i*		0.77457	0.73880	-0.03457	0.0225
C26	2*i*		0.78006	0.73703	0.01761	0.0265

Atom	Wyck.	Occ.	x	y	z	U
C27	2*i*		0.86877	0.78800	0.04710	0.0247
C28	2*i*		0.94750	0.83851	0.02481	0.0452
C29	2*i*		0.93544	0.83821	-0.02758	0.0369
C30	2*i*		0.88160	0.68416	0.11760	0.0262
C31	2*i*		0.88155	0.67629	0.17243	0.0209
C32	2*i*		0.88328	0.76807	0.20601	0.0229
C33	2*i*		0.88332	0.86162	0.18821	0.0281
C34	2*i*		0.87640	0.87321	0.13338	0.0298
C35	2*i*		0.88727	0.58450	0.19064	0.0284
C36	2*i*		0.88210	0.57645	0.24317	0.0317
C37	2*i*		0.86972	0.65864	0.27697	0.0302
C38	2*i*		0.88420	0.75926	0.25853	0.0221
C39	2*i*		0.90736	0.84952	0.29352	0.0311
C40	2*i*		0.89519	0.94322	0.27429	0.0332
C41	2*i*		0.88607	0.95200	0.22222	0.0294
C42	2*i*		0.84547	0.65759	0.32847	0.0318
C43	2*i*		0.88781	0.74277	0.36443	0.0348
C44	2*i*		0.93553	0.83586	0.34689	0.0288
C45	2*i*		0.77751	0.57983	0.34677	0.0472
C46	2*i*		0.76713	0.57871	0.40040	0.0458
C47	2*i*		0.82736	0.65301	0.43491	0.0401
C48	2*i*		0.88694	0.73859	0.41730	0.0327
C49	2*i*		0.94944	0.81347	0.45195	0.0334
C50	2*i*		1.01358	0.89175	0.43454	0.0384
C51	2*i*		1.00682	0.89911	0.38208	0.0306

Atom	Wyck.	Occ.	x	y	z	U
C52	2*i*		0.81854	0.65095	0.48879	0.0432
C53	2*i*		0.94656	0.81023	0.50655	0.0420
C54	2*i*		0.86984	0.73061	0.57564	0.0365
C55	2*i*		0.77740	0.75898	0.59398	0.0399
C56	2*i*		0.77269	0.76406	0.64621	0.0314
C57	2*i*		0.95041	0.71444	0.60883	0.0382
C58	2*i*		0.93921	0.72334	0.65931	0.0289
N60	2*i*		1.32612	1.01998	0.00934	0.0889
C61	2*i*		1.36133	1.03134	0.06337	0.0967
C62	2*i*		1.39421	1.08252	-0.02567	0.1929
C63	2*i*		1.23737	0.96509	-0.01024	0.0840
O64	2*i*		1.18791	0.90538	0.01043	0.1456
N70	2*i*	0.5	0.68747	0.93152	0.42048	0.0578
C71	2*i*	0.5	0.65865	0.91841	0.36701	0.0795
C72	2*i*	0.5	0.74678	1.03662	0.43769	0.0932
C73	2*i*	0.5	0.65524	0.85498	0.44268	0.0972
O74	2*i*	0.5	0.70465	0.86883	0.49524	0.1734
N80	2*i*	0.5	0.52725	0.59590	0.14007	0.0608
C81	2*i*	0.5	0.60057	0.55428	0.17889	0.1035
C82	2*i*	0.5	0.42274	0.53955	0.13137	0.1207
C83	2*i*	0.5	0.56884	0.67655	0.11712	0.0646
O84	2*i*	0.5	0.66075	0.71054	0.12235	0.0565
N90	2*i*	0.5	0.60161	1.00392	0.62161	0.1226
C91	2*i*	0.5	0.62110	1.00945	0.67099	0.1024
C92	2*i*	0.5	0.62340	1.05339	0.58504	0.1175

Atom	Wyck.	Occ.	x	y	z	U
C93	2*i*	0.5	0.55535	0.90111	0.60441	0.1199
O94	2*i*	0.5	0.53542	0.82531	0.62780	0.0984
O20W	2*i*	0.5	0.53691	0.63454	-0.02998	0.0835
C02H	2*i*		0.92411	0.45895	-0.00563	0.1480

Anisotropic displacement parameters (in Å ^{2})

Atom	U_{11}	U_{22}	U_{33}	U_{12}	U_{13}	U_{23}
ZN1	0.02021	0.01289	0.01080	0.00570	0.00525	0.00820
ZN2	0.02462	0.01313	0.01090	0.00479	0.00537	0.00259
CL1	0.11448	0.01678	0.03321	0.00732	0.00098	0.00626
CL2	0.10678	0.01511	0.02151	0.00996	0.01689	0.00222
CL3	0.10065	0.05039	0.02694	-0.03921	0.00792	0.00165
CL4	0.06942	0.03690	0.02803	-0.02166	0.01121	0.00478

Figure A-1: A picture of a ruler was taken under the same magnification as the MOFs in Figure 2.1 to calibrate the I mm length scale

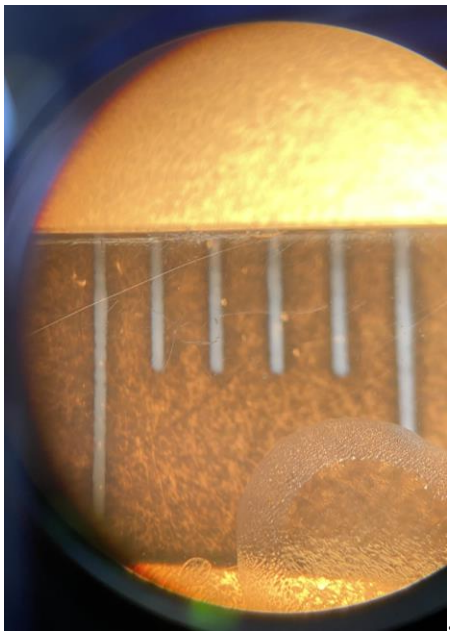 .

Figure A-2: PDIPW 1 Viewed Along Each Axis and Pi-Stacking Distance Calculation

The distances between the pi-conjugated ligands in Figure 2.3 were calculated by copying the packed unit cell (along the b-axis) from Mercury 4.0.0 to Microsoft Paint. A perpendicular (vertical) line was drawn from the center of an ac corner to center of the other c-axis to make a right triangle consisting of the drawn line, a-axis (hypotenuse), and the small portion of the c-axis (spanning from the intersect of the c-axis and drawn line to the closest ac corner. The relative length of the drawn line was calculated by first taking the difference in the pixels' y-coordinates of the ends of the line. The relative length of the other non-hypotenuse side was measured by taking the difference in the x-coordinates. The relative distances were then calculated by using Pythagorean theorem to get the relative hypotenuse length. The actual a-axis length from XRD was then used to get the actual distance of the drawn line. The pi coordinations happen parallel to the alpha plane so the drawn line can be used a reference to calculate the distance between aromatic systems. Two unit cells were stacked on top of each other calculate the distance between the actual pi-stacking, not shown in the unit cell.

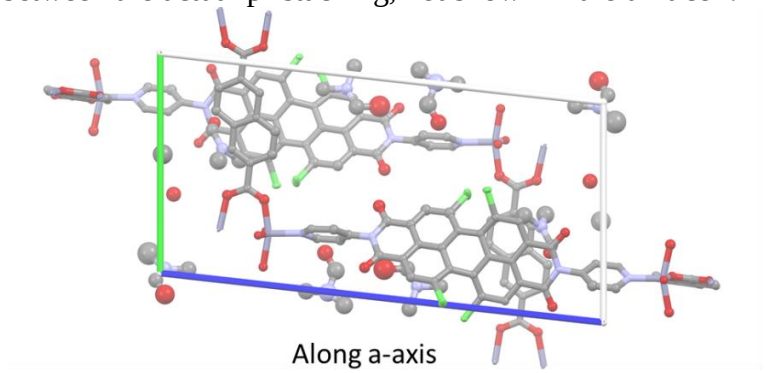

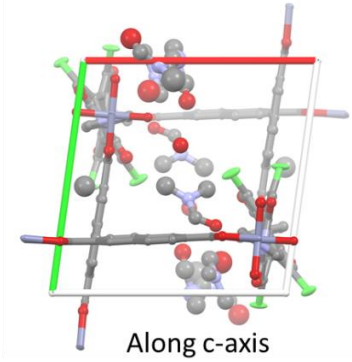

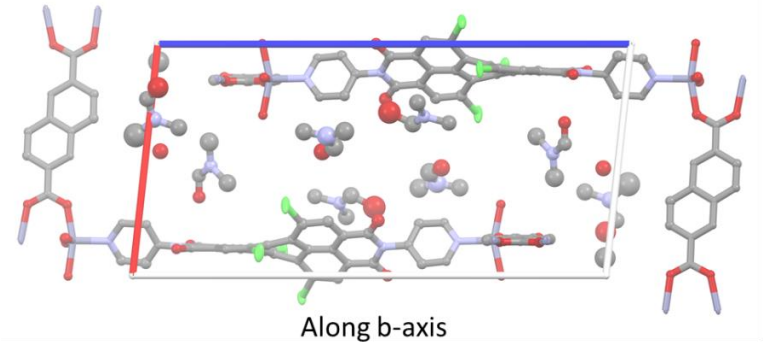

	Triclinic
Space Group	P-1
a	13.0594(13)
b	13.1125(13)
c	26.538(2)
α	95.58(0)
β	95.46(0)
γ	97.16(0)

Figure A-3: PXRD of Reddish, Monolayer-like Surface from Attempted growing of PDIPW 1 on TiO_2-FTO. The 3-point smoothing was done in Microsoft Excel by each intensity data point with its neighboring values. Naturally, the first and last data point must be emitted, explaining the drop to 0 at 40 (2θ)

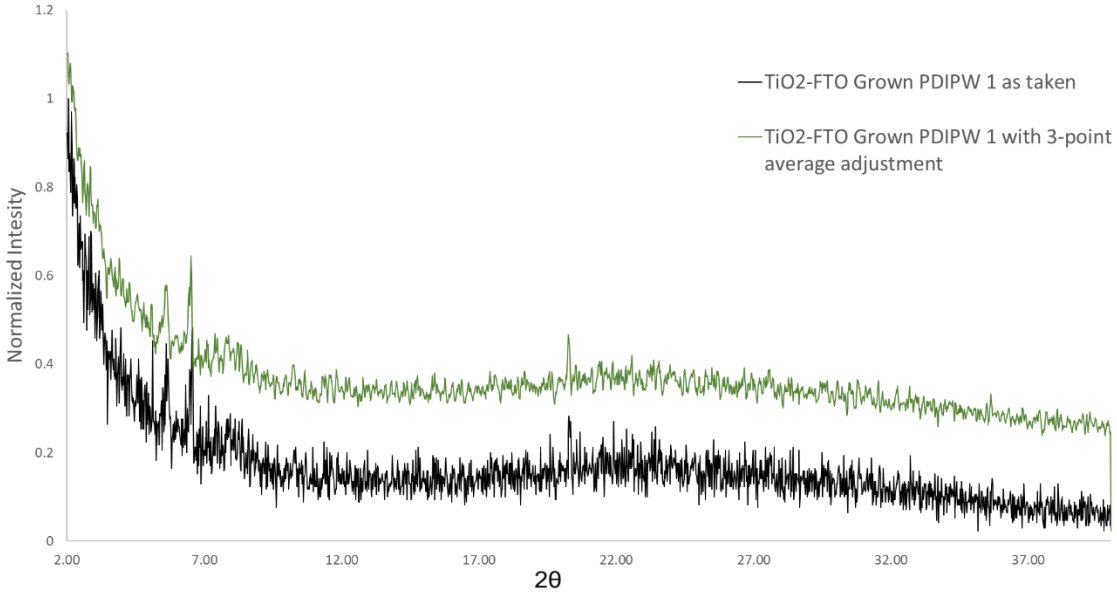

Figure A-4: KB Transform and General Abs Spectra. Green is DR abs of grown **PDIPW 1** on FTO-TiO_2.Yellow is the DR abs of blank FTO-TiO_2. Blue is the abs of DC **PDIPW 1** FTO-TiO_2

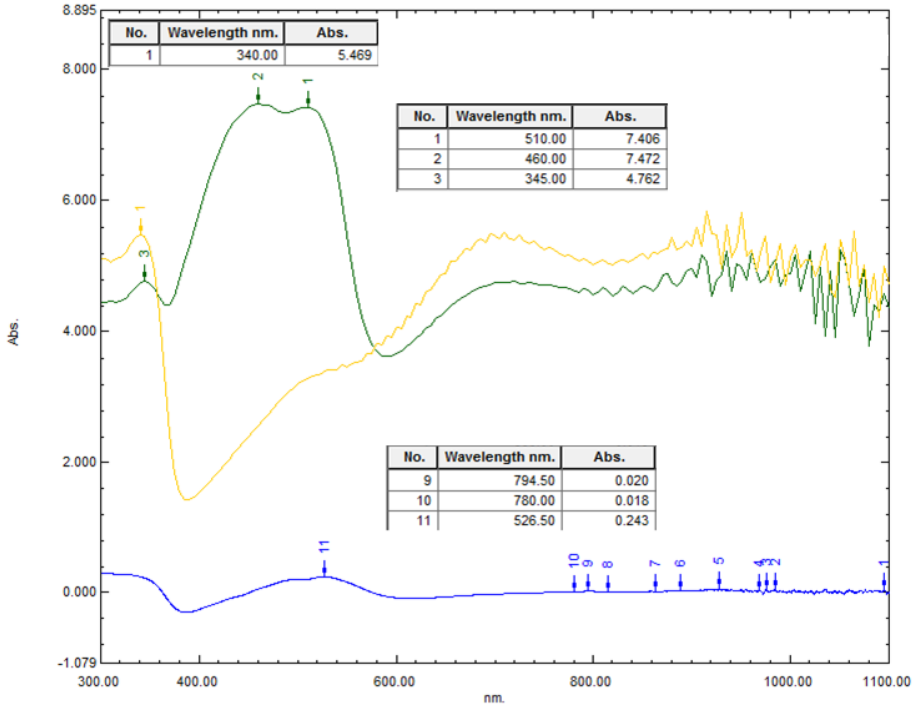

Appendix B

H-NMR and MALDI-TOF Characterization

Figure B-1: H-NMR of n-octylPDICl$_4$

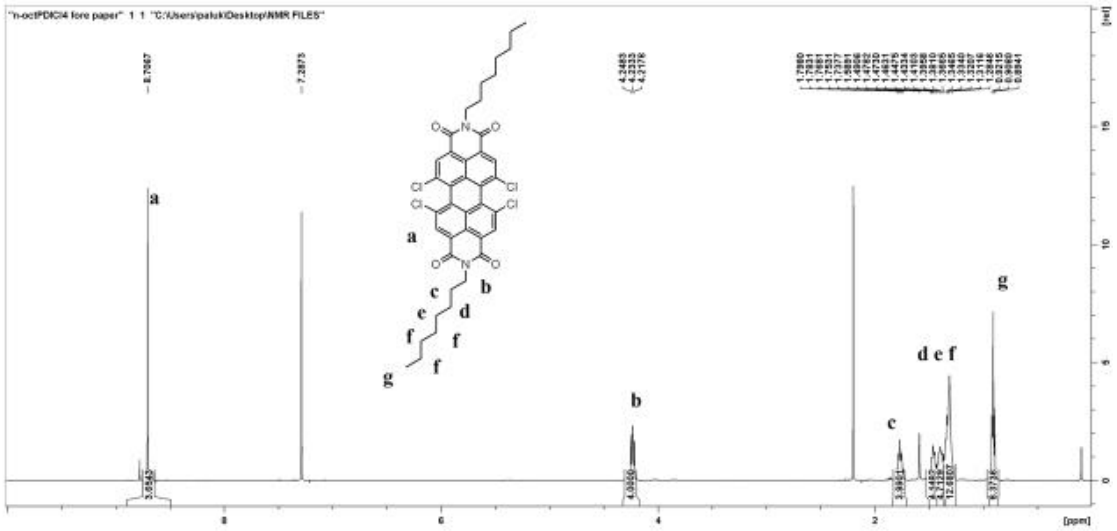

Figure B-2: H-NMR of BPyPDICl$_4$

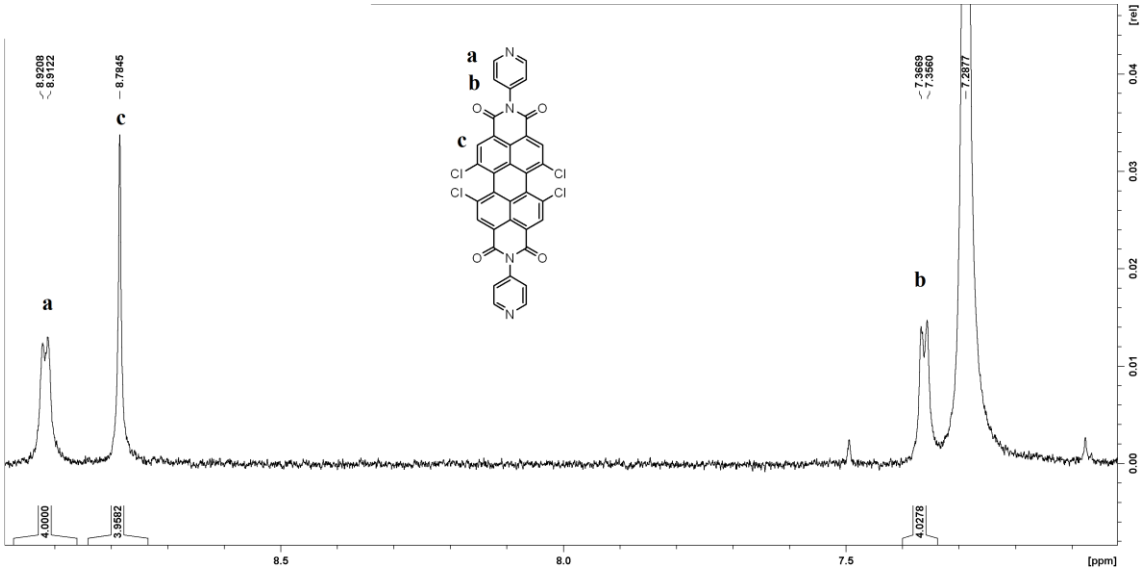

Figure B-3: H-NMR of t-butPDICl$_4$

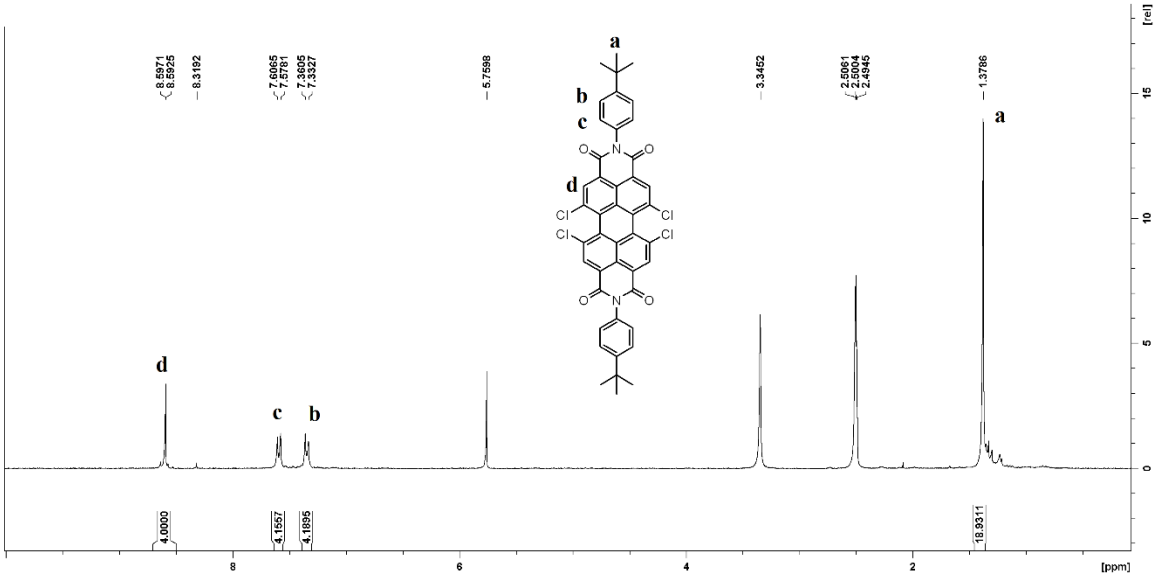

Figure B-5: H-NMR of tetra-substituted 2-methoxyethanol BPyPDICl$_4$

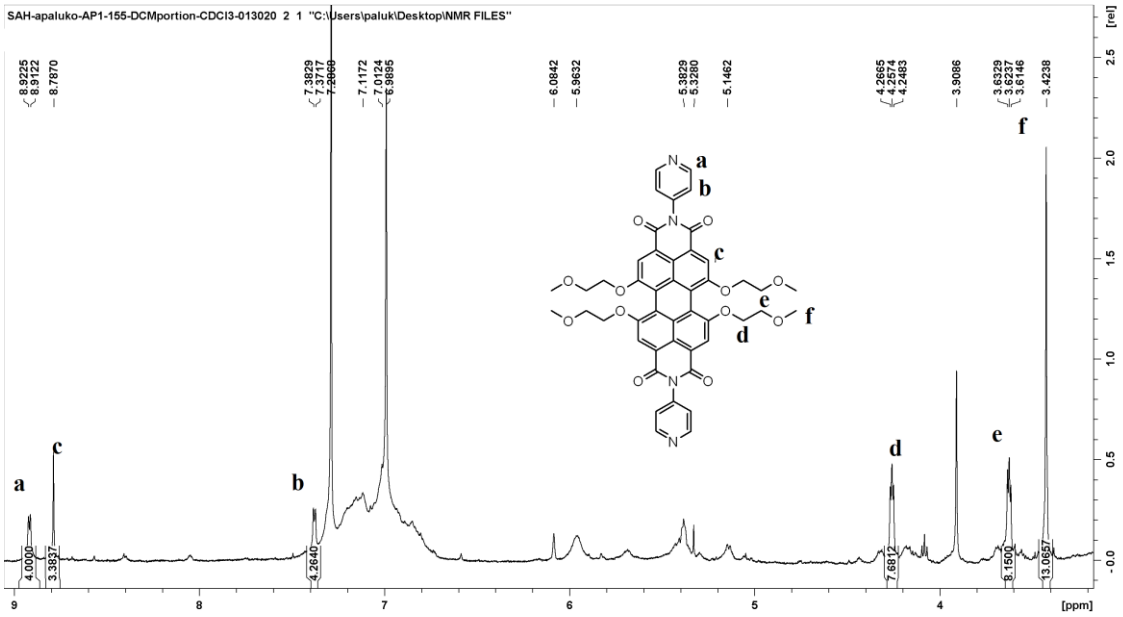

Figure B-6: MALDI-TOF of n-octylPDICl$_4$

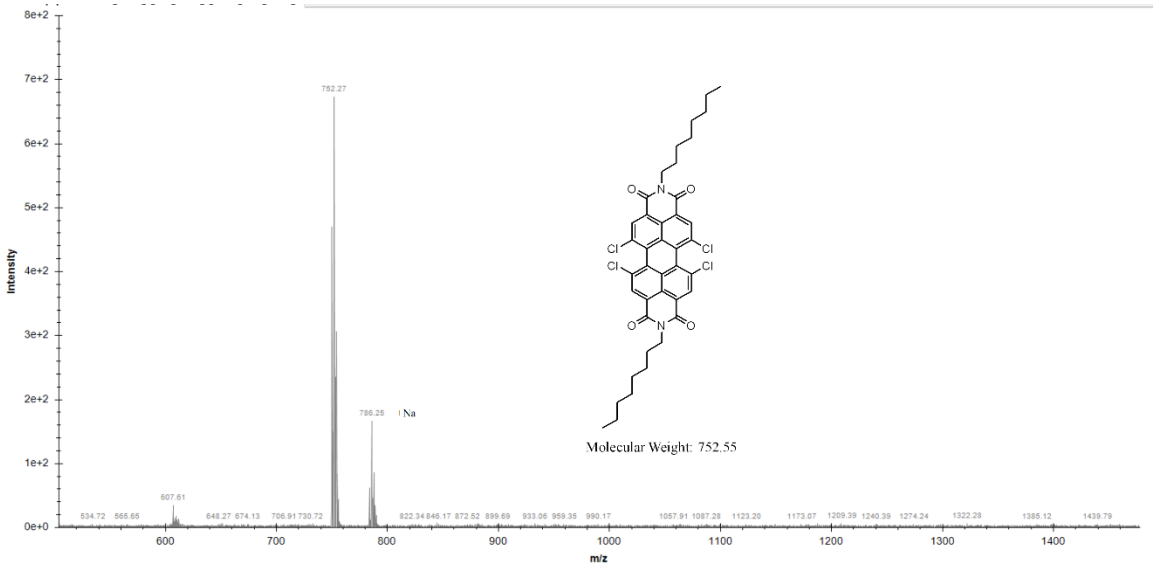

Figure B-7: MALDI-TOF of BPyPDICl$_4$

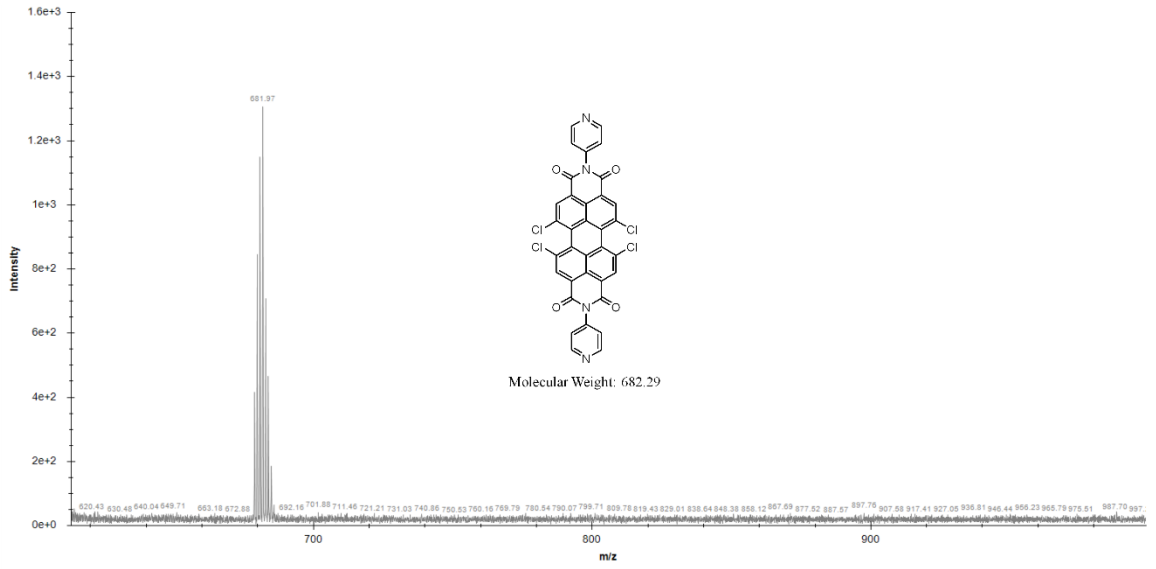

Figure B-8: MALDI-TOF of t-butPDICl$_4$

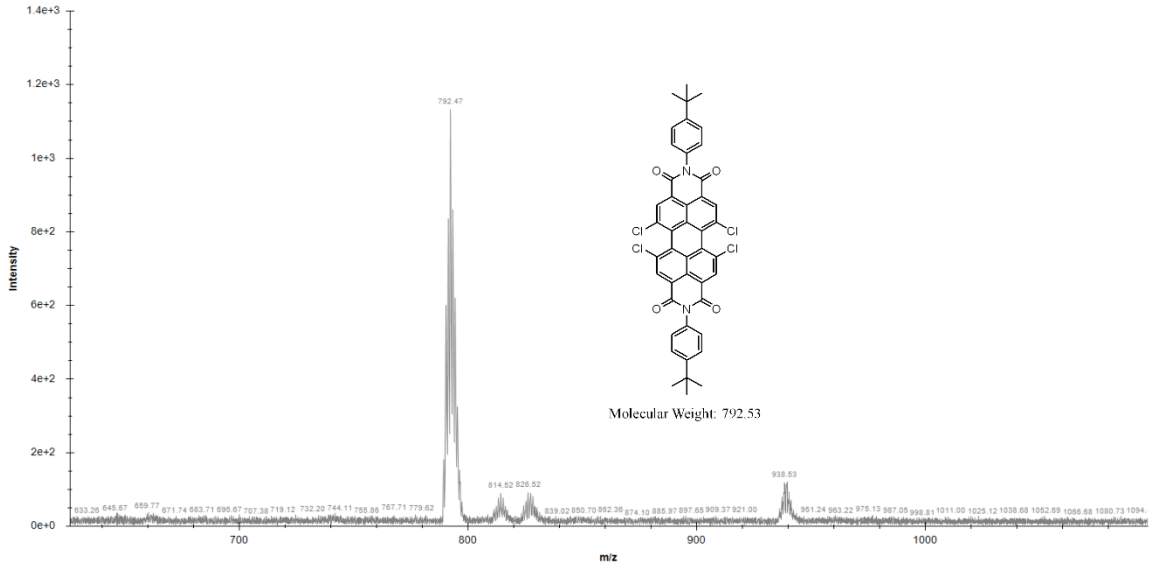

Figure B-9: MALDI-TOF of n-octPDI CH

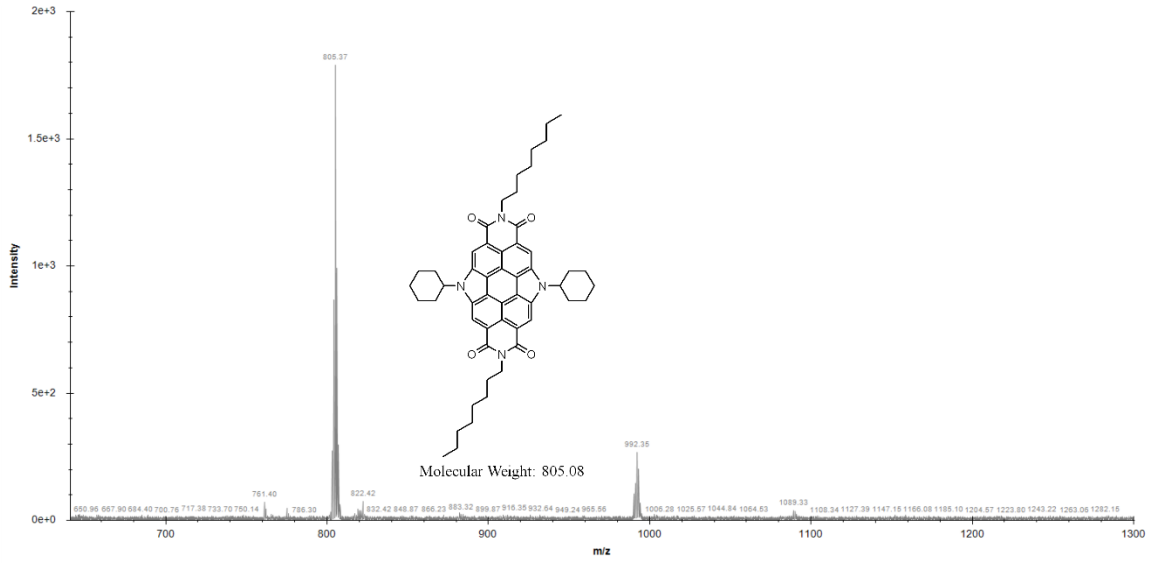

Figure B-10: MALDI-TOF of n-octPDI DMH

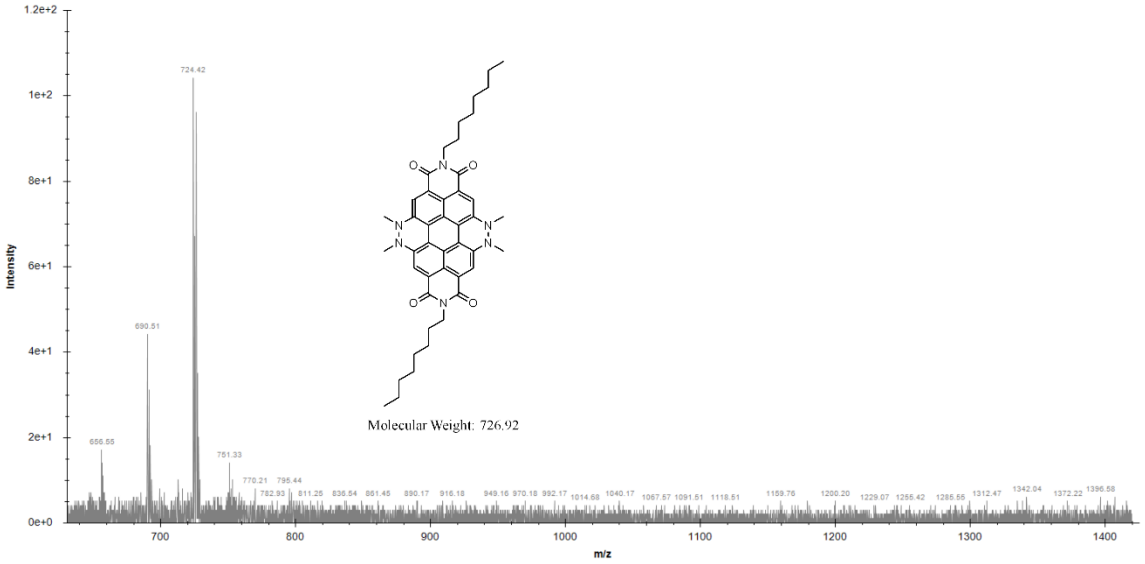

Figure B-11: MALDI-TOF of n-octPDI pyrrolidne

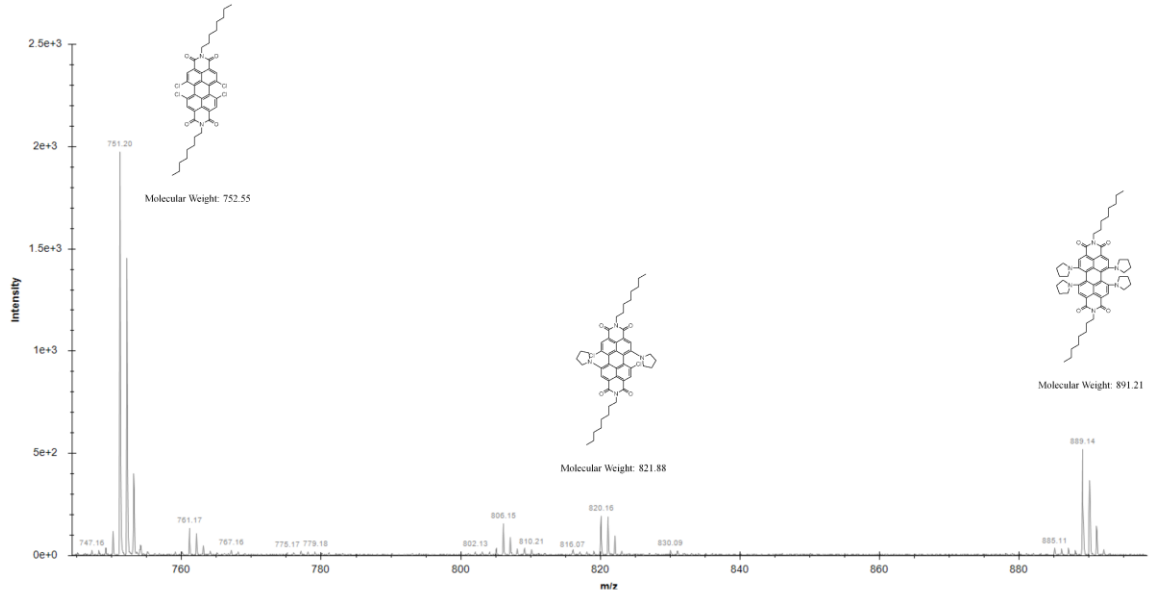

Figure B-12: MALDI-TOF of BPyPDICl$_4$ methoxyethanol

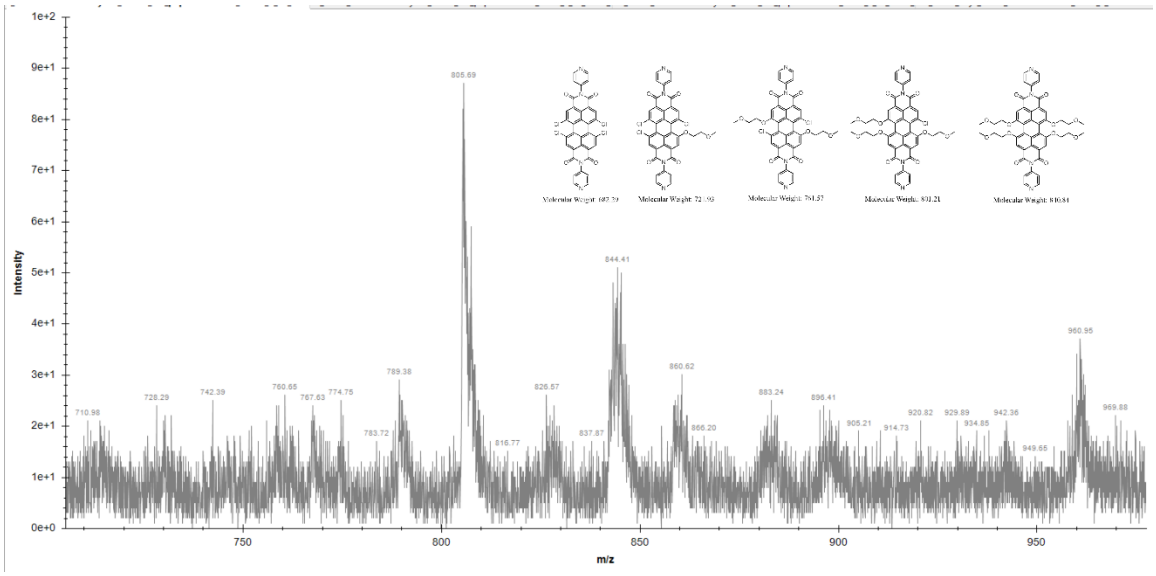

Figure B-13: MALDI-TOF of n-octPDI methoxyethanol

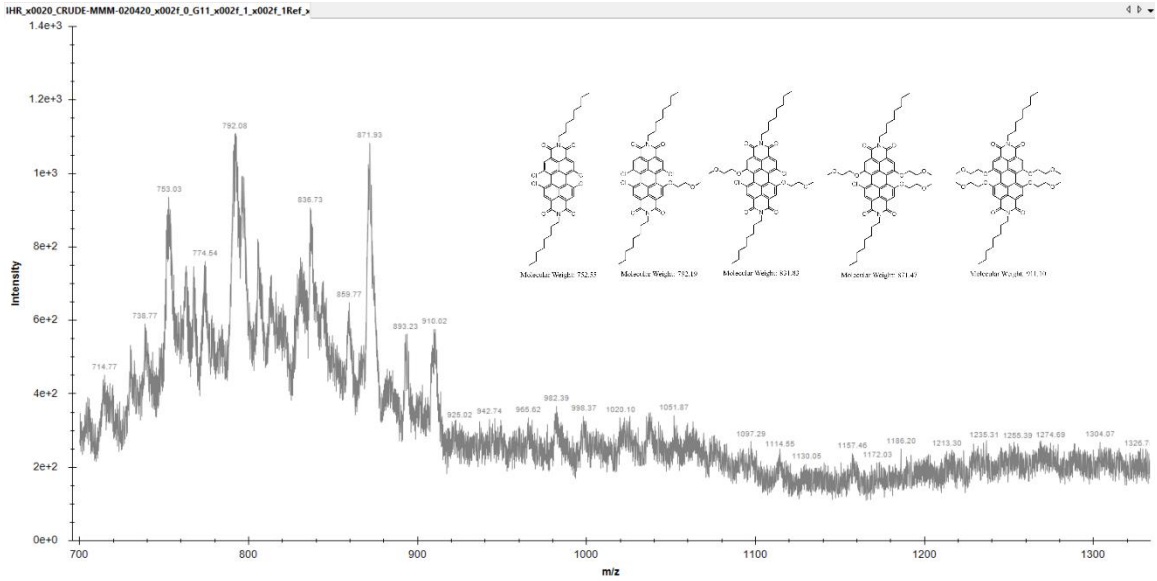

Figure B-14: MALDI-TOF of n-octPDI pentaethelene glycol

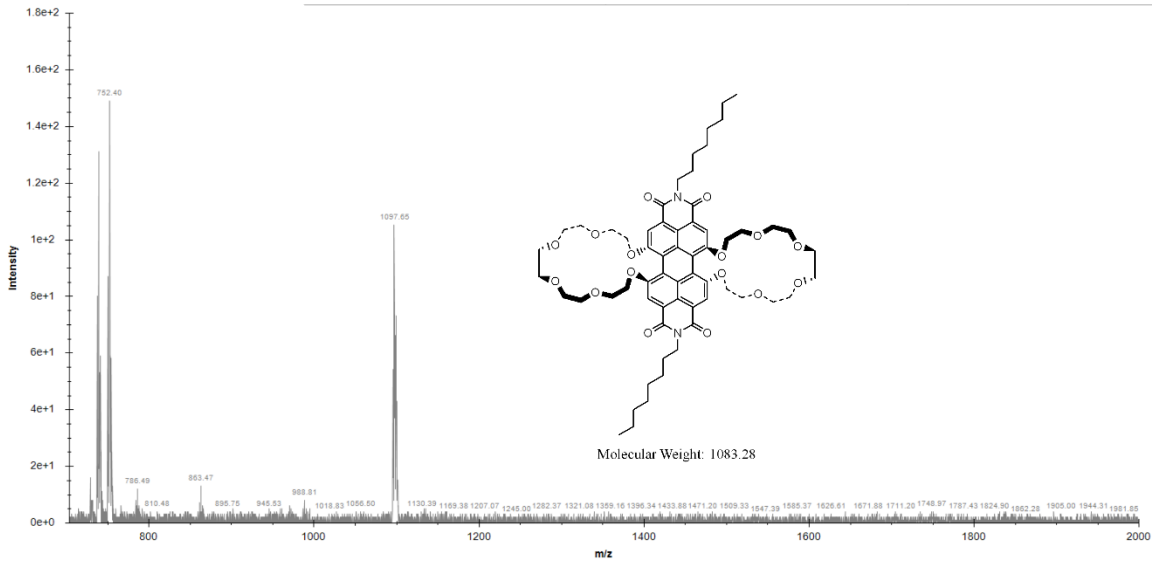

Figure B-15: H-NMR of TCPP (bottom) and Pt TCPP (TOP)

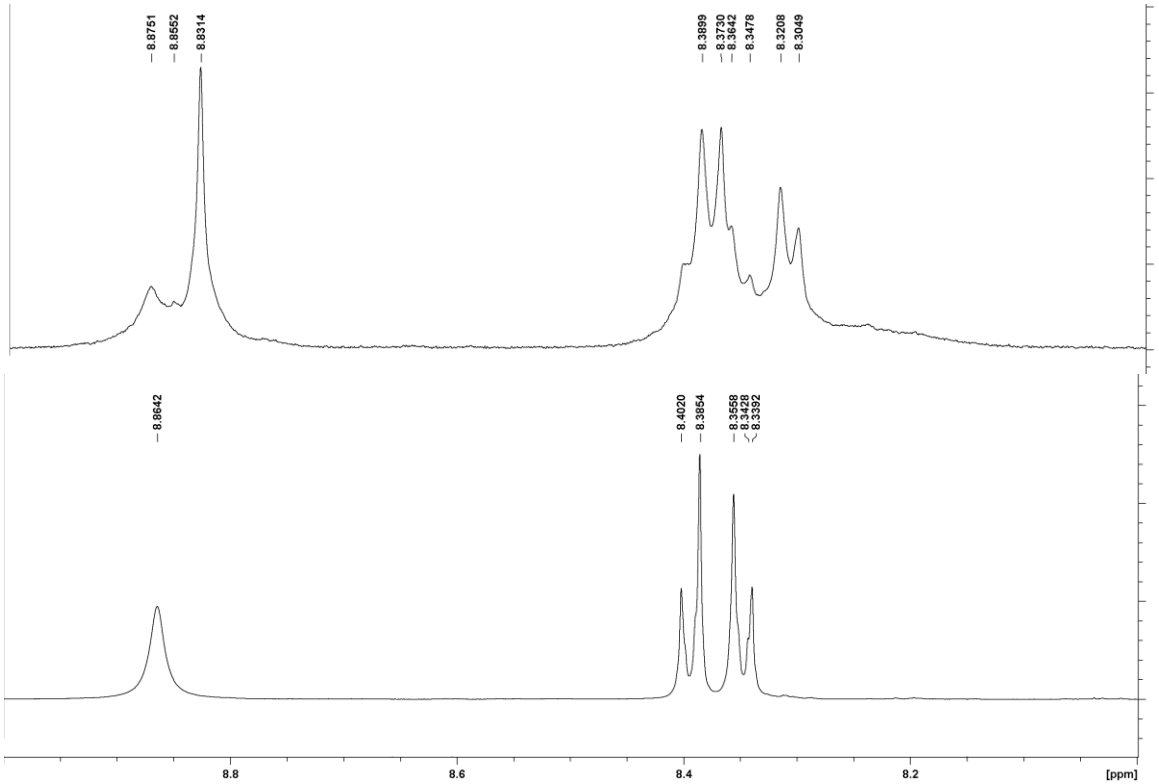

Figure B-15: MALDI-TOF of TCPP (+Pt)